



ELSEVIER

Contents lists available at ScienceDirect

Combustion and Flame

journal homepage: www.elsevier.com/locate/combustflame

A comprehensive experimental and kinetic modeling study of di-isobutylene isomers: Part 1

Nitin Lokachari^a, Goutham Kukkadapu^b, Hwasup Song^{c,1}, Guillaume Vanhove^c, Maxence Lailliau^d, Guillaume Dayma^d, Zeynep Serinyel^d, Kuiwen Zhang^b, Roland Dauphin^e, Brian Etz^f, Seonah Kim^{f,g}, Mathias Steglich^h, Andras Bodi^h, Gina Fioroni^f, Patrick Hemberger^h, Sergey S. Matveevⁱ, Alexander A. Konnov^j, Philippe Dagaut^d, Scott W. Wagon^{b,*}, William J. Pitz^b, Henry J. Curran^a

^a Combustion Chemistry Centre, School of Chemistry, Ryan Institute, MaREI, National University of Ireland Galway, Ireland

^b Lawrence Livermore National Laboratory, Livermore, CA 94551, USA

^c Univ. Lille, CNRS, UMR 8522 PC2A Physicochimie des Processus de Combustion et de l'Atmosphère, Lille F, 59000, France

^d CNRS-INSIS, Institut de Combustion, Aérodynamique, Réactivité et Environnement (ICARE), Orléans, France

^e TotalEnergies OneTech, Centre de Recherche de Solaize, Chemin du Canal BP 22, Solaize 69360, France

^f National Renewable Energy Laboratory, Golden, CO 80401, USA

^g Department of Chemistry, Colorado State University, Fort Collins, CO 80523, USA

^h Laboratory for Synchrotron Radiation and Femtochemistry, Paul Scherrer Institute, Villigen 5232, Switzerland

ⁱ Scientific and Educational Centre of Fluid Dynamics Research, Samara National Research University, Samara, Russia

^j Division of Combustion Physics, Lund University, Lund, Sweden

ARTICLE INFO

Article history:

Received 9 September 2021

Revised 12 July 2022

Accepted 13 July 2022

Available online xxx

Keywords:

Di-isobutylene

Chemical kinetics

Rapid compression machine

Jet-stirred reactor

Kinetic modeling

ABSTRACT

Di-isobutylene has received significant attention as a promising fuel blendstock, as it can be synthesized via biological routes and is a short-listed molecule from the Co-Optima initiative. Di-isobutylene is also popularly used as an alkene representative in multi-component surrogate models for engine studies of gasoline fuels. However, there is limited experimental data available in the literature for neat di-isobutylene under engine-like conditions. Hence, most existing di-isobutylene models have not been extensively validated, particularly at lower temperatures (< 1000 K). Most gasoline surrogate models include the di-isobutylene sub-mechanism published by Metcalfe et al. [1] with little or no modification. The current study is undertaken to develop a detailed kinetic model for di-isobutylene and validate the model using a wide range of relevant experimental data. Part 1 of this study exclusively focuses on the low- to intermediate temperature kinetics of di-isobutylene. An upcoming part 2 discusses the high-temperature model development and validation of the relevant experimental targets. Ignition delay time measurements for the di-isobutylene isomers were performed at pressures ranging from 15 – 30 bar at equivalence ratios of 0.5, 1.0, and 2.0 diluted in air and in the temperature range 650 – 900 K using two independent rapid compression machine facilities. In addition, measurements of species identified during the oxidation of these isomers were performed in a jet-stirred reactor and in a rapid compression machine. A detailed kinetic model for the di-isobutylene isomers is developed to capture the wide range of new experimental targets. For the first time, a comprehensive low-temperature chemistry submodel is included. The differences in the important reaction pathways for the accurate prediction of the oxidation of the two DIB isomers are compared using reaction path analysis. The most sensitive reactions controlling the ignition delay times of the DIB isomers under the pressure and temperature conditions necessary for autoignition in engines are identified.

Published by Elsevier Inc. on behalf of The Combustion Institute.

* Corresponding author at: Lawrence Livermore National Laboratory, Livermore, CA 94551, United States.

E-mail address: Wagon1@llnl.gov (S.W. Wagon).

¹ Present address: Department of Mechanical Engineering, Kumoh National University of Technology, 61 Daehak-ro, Gumi, Gyeongsangbuk-do, 39,177, Korea.

1. Introduction

The Co-Optimization of fuels and engines (Co-Optima) initiative identified fuel properties of blendstocks that can increase the engine efficiency of boosted, spark-ignition (SI) engines when added to a petroleum based fuel [1,2]. Boosted SI engines operate at

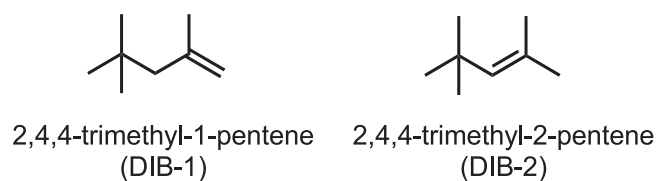


Fig. 1. A two-dimensional representation of DIB isomers.

higher in-cylinder pressures. Therefore, they require fuels with higher research octane number (RON), octane sensitivity (S), and heat of vaporization (HOV) to avoid undesirable engine knock [3]. A comprehensive evaluation of more than 400 blendstocks from a variety of chemical families, which can also be sourced from biomass [4], followed by a rigorous screening, led to the identification of six blendstocks with fuel properties that, when used in boosted SI engines, can reduce environmental impacts and offer better engine efficiency. Six short-listed fuel blendstocks, with the fewest significant practical barriers for scale-up and commercialization, have been identified as: di-isobutylene (DIB), ethanol, isobutanol, *n*-propanol, *iso*-propanol, and a fusel alcohol blend. This study focuses on investigating the auto-ignition characteristics of DIB.

DIB is a branched alkene (contains one C=C) with an alkyl substitution on the double bond (see Fig. 1) and is often referred to as a mixture of its two isomers 2,4,4-trimethyl-1-pentene (DIB-1) and 2,4,4-trimethyl-2-pentene (DIB-2). Commercially available DIB is generally a mixture of the two isomers with 75% DIB-1 and 25% DIB-2. DIB has attractive fuel properties for boosted SI engines, such as a high RON and octane sensitivity [3]. DIB can be prepared through the dimerization of isobutene, which can be synthesized from bio-derived alcohols, ethanol, or *iso*-butanol [3]. In addition, the DIB isomers received significant attention as simple representatives of alkene compounds in multi-component surrogate fuels [1,5–13], which are often formulated to contain one or more representative components from various classes of compounds, including alkanes, alkenes, aromatics, etc., to represent a complex commercial fuel and to simulate real fuels in multi-dimensional simulations of engine combustion.

In addition to their use in surrogate fuels, studying the DIB isomers offers kinetic insights into the effect of the presence of an unsaturated bond in *iso*-octane. Alkenes are key intermediates formed during the oxidation of heavier saturated hydrocarbons and constitute a significant portion of commercial transportation fuels. Short-chained alkenes are known to have much higher knock resistance than their alkane counterparts [14]. However, in contrast to alkanes, the combustion kinetics of alkenes are less well studied and understood.

Moreover, most gasoline surrogate models include the DIB-1 sub-mechanism published by Metcalfe et al. [1] which was only validated for temperatures above 1200 K and did not include key reaction pathways relevant to low-temperature combustion. Moreover, experimental ignition delay times (IDTs) for neat DIB-1 are limited to low pressures and high temperatures. Metcalfe et al. [1] reported IDT experiments at low fuel concentrations (0.375% and 0.75%) in the temperature range 1200 – 1500 K and at pressures of 1 – 4 atm. Hu et al. [8] conducted IDT experiments for neat DIB-1 at fuel concentrations ranging from 0.5 – 1.0%, at temperatures in the range 1110 – 1500 K, and at pressures in the range of 2 – 10 atm. For experiments where DIB-1 is included as a surrogate component in a mixture, Mittal and Sung [15] performed IDT experiments in an RCM in the temperature range 750 – 1050 K and at pressures of 35 and 45 atm. More recently, high pressure (15 – 30 atm) and low to intermediate temperature (650 – 1000 K) DIB studies were carried out in a rapid compression machine (RCM)

Table 1

List of experimental conditions and the molar composition of the test fuel/oxidizer composition studied for DIB-1.

Φ	Fuel (%)	O ₂ (%)	N ₂ + Ar (%)	Compressed pressure (bar)
0.5	0.87	20.82	78.31	15, 30
1.0	1.72	20.64	77.64	15, 20, 25, 30
2.0	3.38	20.29	76.33	15, 30

[16,17]. Due to the limited data available at low temperatures and high pressures, most literature multi-component gasoline surrogate models have not been extensively validated for the DIB isomers at engine-relevant pressures and temperatures.

To motivate the current work, simulated results from kinetic models in the literature are compared to the new experimental IDT data presented in Fig. 2. The models proposed by Metcalfe et al. [1] and Li et al. [9] are in relatively good agreement with the new experimental data in the temperature range 900 – 1350 K, while poor quantitative predictions are observed for several multi-component surrogate models. Due to the lack of comprehensive low-temperature oxidation (LTO) chemistry and lack of knowledge about the DIB allylic radical decomposition reactions, most of the multi-component surrogate models considered for this study could not reproduce the new experimental data over the entire temperature range investigated in Fig. 2. Recently, Lokachari et al. [18] highlighted the significant hierarchical dependence of the DIB-1 oxidation mechanism on the underlying isobutene kinetics, which is a critical intermediate formed in the decomposition of DIB-1, particularly at high temperatures (> 1000 K). The influence of isobutene kinetics on the predictions of IDTs and laminar burning velocities (LBVs) for DIB-1 oxidation has also been reported recently by Lokachari et al. [18] and it was concluded that isobutene kinetics largely controls the high temperature oxidation of DIB-1.

The development of a comprehensive chemical kinetic mechanism for the DIB isomers and its validation using a wide range of reliable experimental targets is the main objective of the current study. This paper (part 1) exclusively focuses on the model development and validation of low to intermediate temperature experimental data of the DIB isomers, using IDT measurements performed in two independent laboratories and speciation data from a jet-stirred reactor (JSR) and RCM are also included in this paper. The upcoming part-2 [19] (in preparation) focusses on the high temperature oxidation chemistry of the DIB isomers using relevant experimental validation datasets from various other fundamental reactors.

2. Experimental methods

To understand the oxidation chemistry and the ignition propensity of DIB, speciation and IDT were conducted in two RCMs and in a JSR. The IDT measurements were acquired using two separate RCM facilities at NUI Galway and ULille. Speciation experiments were performed in an RCM at ULille and in a JSR at ICARE Orléans. The details of the conditions of the experiments performed are listed in Tables 1–3.

2.1. Rapid compression machine (NUIG)

The RCM at NUIG is employed to complement the high-pressure shock tube (HPST) experiments to measure IDTs in the low to intermediate temperature regime (650 – 900 K), with the experimental details provided in Table 1. The test fuel (DIB-1 98.5%) was supplied by Sigma Aldrich®. The other gases used in this study, nitrogen (99.99%), oxygen (99.99%), argon (99.96%), and helium (99.97%), were purchased from BOC Ireland. Homogeneous fuel-air

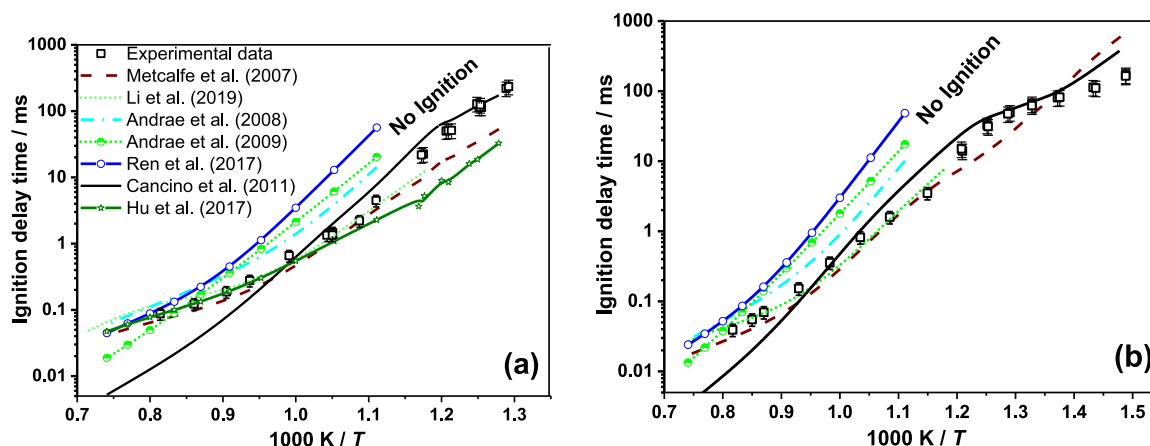


Fig. 2. Validation of literature multi-component surrogate models against new DIB-1 IDT experiments (open squares) performed in the shock-tube and rapid compression machine at NUIG for fuel in air mixtures at $\varphi = 1.0$ and (a) $pc = 15$ and (b) $pc = 30$ bar.

Table 2

List of experimental conditions studied at ULille RCM for DIB-1 and DIB-2 IDTs at $\varphi = 1.0$ and 15, 20 and 25 bar in the range of $T_c = 660 - 900$ K.

DIB (%)	O ₂ (%)	N ₂ (%)	Ar (%)	CO ₂ (%)
1.72	20.64	0.00	77.63	0.00
1.72	20.64	6.99	70.64	0.00
1.72	20.64	13.20	64.40	0.00
1.72	20.64	20.96	56.67	0.00
1.72	20.64	29.50	48.13	0.00
1.72	20.64	38.82	38.82	0.00
1.72	20.64	46.58	31.05	0.00
1.72	20.64	54.34	23.30	0.00
1.72	20.64	62.11	15.53	0.00
1.72	20.64	69.87	7.76	0.00
1.72	20.64	77.63	0.00	0.00
1.72	20.64	71.42	0.00	6.20

mixtures were prepared in an external stainless-steel vessel maintained at ~ 50 °C to prevent fuel condensation and to permit the fuel and air to diffusively mix for at least 12 h before performing the experiments. The RCM has an opposed twin-piston arrangement with a 38 mm bore and a 168 mm stroke. Briefly, the premixed fuel/air mixture is introduced into the reaction chamber and is rapidly compressed (~ 16 ms) by the pistons. Creviced piston heads are used to largely limit turbulence/roll-up vortices generated in the test gas. The pistons are pneumatically driven and locked at the end of compression, creating a constant volume condition. After compression, the pressure drops due to heat loss from the gas mixture to the reaction chamber walls. Thus, to isolate the heat-transfer effects, pyrolytic (non-reactive) pressure profiles are recorded by replacing O₂ with N₂ to account for these effects in the simulations.

A range of compressed gas temperatures is obtained by varying the initial temperature of the RCM system to temperatures not greater than 150 °C, to avoid damaging the seals within the system. To further achieve higher compressed temperatures, a 50% N₂/50% Ar diluent ratio was used. IDTs and compressed pressures are mea-

sured using a Kistler 603CAB sensor mounted on the sidewall of the reaction chamber. The ‘adiabatic compression/expansion’ routine in Gaseq [20] is used to calculate the compressed temperature. The representative experimental pressure traces for DIB isomers are depicted in Fig. 3. The overall uncertainty in IDT and the compressed temperature are estimated to be about 25% and ± 7 K respectively. A summary of the NUIG experimental test matrix is shown in Table 1, and more detailed information on the composition, inlet pressure, inlet pressure along with the volume histories are provided in the Supplementary material.

2.2. Rapid compression machine (ULille)

The ULille RCM has been utilized for decades to measure IDTs of a wide variety of fuels, as well as to perform speciation measurements to track the evolution of the stable species formed during the ignition delay period and to provide direct kinetic insights to construct and validate a reaction mechanism, as demonstrated in recent studies [21–23]. The driving piston, which is run by compressed air and stopped by hydraulics, and the driven piston are connected at a right angle on the same plane by a grooved metallic cam. The advantages of this design are that the compression-time history is reproducible with repeated experiments and that the piston rebound at the end of compression is suppressed as the grooved section of the cam holds the driven piston at its top dead centre (TDC) position. In addition, the driven piston is equipped with a creviced piston head [24] to maintain temperature homogeneity after the compression phase by absorbing the thermal boundary layer developed during the compression stroke by suppressing roll-up vortex formation [25,26]. With a 50 mm bore and 200 mm stroke, the combustion chamber is heated by multiple electric band heating elements. The axial deviation of the in-cylinder temperature is carefully adjusted to remain within 1 K, which leads to a maximum compressed temperature deviation of 2 – 2.5 K, depending on the mixture composition. The compression ratio is adjustable by installing different end plates at the top of the combustion chamber to modify the clearance height and was

Table 3

Experimental conditions investigated in the JSR.

Equivalence ratio (φ)	0.5, 1.0 and 2.0	0.5 and 1.0
Test mixture composition	1000 ppm neat DIB-1	750 ppm DIB-1 + 250 ppm DIB-2
Residence time (τ)	0.7 s	0.7 s
Pressure (p)	10 atm	10 atm
Temperature (T)	700 – 1200 K	700 – 1200 K

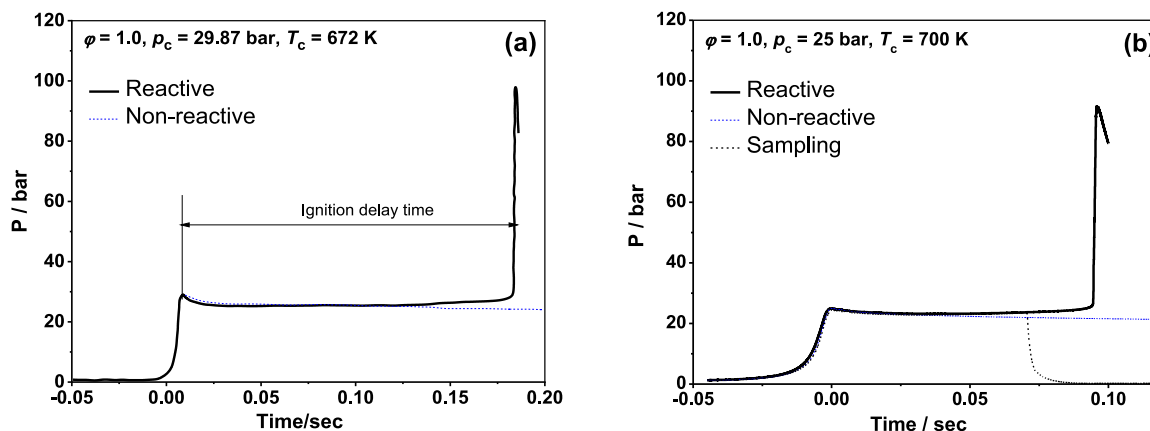


Fig. 3. Representative RCM pressure traces measured (a) DIB-1 at NUIG and (b) DIB-2 at ULille.

fixed at 10.3 for this work. A thermal shock-protected piezoelectric pressure transducer (Kistler 601CA) was coupled with a charge amplifier (Kistler 5007) to record the pressure-time history during the experiments. For the mixture preparation, high purity DIB isomers, i.e., DIB-1 (> 99%, Acros Organics) and DIB-2 (> 98%, Acros Organics), were treated with repeated freeze-thaw distillation to remove any dissolved gases, and all the gaseous components, i.e., Ar, N₂, and O₂, were supplied by Air Liquide (≥ 99.99%). The overall uncertainty in IDT and the compressed temperature are estimated to be about 25% and ± 5 K, respectively.

In addition, sampling and speciation experiments were conducted to provide detailed experimental evidence to validate the DIB kinetic model by observing the formation of stable intermediates at $T_c = 700 \pm 2$ K, $p_c = 25 \pm 0.5$ bar, and $\phi = 1.0$. Comparing the speciation results from the isomers helps to develop their kinetic models, especially when their structure-specific intermediates are expected in large quantities. For example, C=C double bond-specific reaction pathways for alkenes at low-to-intermediate temperatures were experimentally validated in previous studies regarding a mixture of DIB-1 and DIB-2 [17] and the linear hexene isomers [27]. Reacting mixture sampling is realized by a sudden expansion of the compressed volume during the ignition delay period, thereby quenching reactions and freezing the composition thanks to the superior volume ratio of 40 (sampling canister) to 1 (the volume of the fully compressed combustion chamber). Samples were taken near 0.84 (for DIB-1) and 0.70 (for DIB-2) of the normalized time of the total IDT at the condition above for each isomer. Once the sample was taken, it was immediately injected into two gas chromatographs (GCs); a primary Bruker Scion 456 equipped with a mass spectrometer (MS), a thermal conductivity detector (TCD), and a flame ionization detector (FID) along with BR-5 and PoraBond-Q columns for the separation of heavy and light hydrocarbons, and a secondary Agilent 6890 with a molecular sieve and TCD/FID for the detection of permanent gases and CO. The effective carbon number (ECN) concept was applied to derive the mole fractions of different intermediates from the FID response signal [28], with an uncertainty estimated to be within ± 15%.

Selectivities of the intermediates were calculated by normalizing the mole fraction of the all the identified intermediates. In detail, the following equation is used,

$$S_i = \frac{x_i}{\sum_{i=1}^N x_i}$$

S_i denotes the selectivity of the i^{th} species and x_i is the mole fraction of the i^{th} species, respectively. Since the maximum achievable TDC pressure is slightly lower than 25 bar when the sampling

apparatus is installed, the relevant IDT at the sampling condition is slightly longer than the corresponding non-sampling condition.

2.3. Jet stirred reactor

The oxidation of DIB (neat DIB-1 and a mixture of 75% DIB-1 and 25% DIB-2 by mole) was carried out in a fused silica JSR at the Institut de Combustion, Aérothermique, Réactivité et Environnement (ICARE). This setup can be used for studies at pressures of up to 10 atm and at temperatures up to 1280 K. The fuel was handled using an HPLC pump, atomized, and vaporized through heated grids in a nitrogen flow and then carried to the reactor by a quartz capillary. The fuel is highly diluted to avoid strong heat release. The oxidizing mixture (N₂+O₂) is conveyed to the reactor separately to avoid any premature reactivity. The two flows meet at the entrance of the injectors and are mixed by high turbulence generated by four nozzles. The temperature is monitored using a Pt-Pt/Rh-10% thermocouple isolated from the gases by a quartz sheath to avoid any catalytic reaction. A low-pressure sonic probe is used to sample the reactor and freeze the reactivity. The samples are then analyzed online by Fourier transform infrared spectroscopy (FTIR) or stored at low-pressure in 1 L Pyrex bulbs for further GC analyses. Off-line analyses were performed using GCs equipped with capillary columns (0.32 mm i.d.: DB-624 and CP-Al2O3-KCl, and 0.53 mm i.d.: CarboPlot-P7), a thermal conductivity detector (TCD), and a flame ionization detector (FID). A GC-MS (Varian quadrupole V1200) operating with electron ionization (70 eV) was used for product identification. More details regarding this setup can be found in the literature [29].

The mole fraction profiles of the reactants (DIB-1, DIB-2, and O₂) and products (H₂, H₂O, CO, CO₂, CH₂O, CH₄, C₂H₄, C₂H₆, C₂H₂, C₃H₆, isobutene, 2-methyl but-1-ene, isoprene, CH₃CHO, acrolein, 2-methyl propanal, methacrolein, acetone, methyl vinyl ketone, and benzene) were measured by FTIR and GC. Uncertainties regarding the results can be attributed to temperature measurements within the reactor (± 5 K), the reactants and diluent flow rates, and the analyses. The total uncertainty in species mole fractions is challenging to quantify but can be estimated to be ± 15%. The elemental balance is checked at the end of each experiment and stays within 10% for carbon and hydrogen, and is within 15% for oxygen.

Experiments were carried out at steady state, at 10 atm pressure, at constant residence time $\tau = 0.7$ s, and at equivalence ratios of 0.5, 1.0, and 2.0 for pure DIB-1, and 0.5 and 1.0 for the DIB mixture. The initial fuel mole fraction was held constant (1000 ppm), and temperatures ranged from 720 – 1200 K in 30 K increments.

3. Kinetic modeling

The chemistry of alkenes at low and intermediate temperatures is more complicated than that for alkanes due to the C=C double bond, as H-atom abstraction can form allylic and vinylic radicals in addition to alkyl-like radicals and the addition of radicals to the double bond need to be considered. The rate constants of many of these C₈ allylic radical decompositions are not well known. Moreover, the low-temperature mechanism describing alkene combustion contains hundreds of species and thousands of elementary reactions, each of which are assigned thermodynamic properties and rate constant expressions, respectively. Unfortunately, there is very little or no experimental data on most of these properties. Thus, kineticists rely primarily on theoretical studies to provide the rate constant and thermodynamic property data for the oxidation of alkenes, and to develop rate rules for various reaction classes necessary to describe alkene low-temperature combustion.

The DIB models have been developed as a collaborative effort between NUIG and LLNL. The small hydrocarbon (C₀ – C₄) base chemistry has been adapted from the recent study by Lokachari et al. [18], while the C₅ and C₆ species chemistry is adopted from Bugler et al. [30] and Zhang et al. [31], respectively. Since the DIB isomers are intermediates formed during the oxidation of iso-octane, the recent iso-octane sub-mechanism is adopted from Fang et al. [32]. The high temperature chemistry of DIB-1 is majorly dependent on an accurate kinetic description of isobutene chemistry, whose kinetic parameters have been re-assessed [18] by incorporating the rates and thermochemical properties from recent advances from ab-initio studies and experimental diagnostics. The description of the kinetic model development below will mainly focus on the key reaction classes. An additional description focusing on the high temperature part of the DIB mechanism is given in Part 2 [19]. In this study, the thermochemical data has been calculated for all of the species of interest to DIB oxidation using Benson's group additivity method using the THERM software [33] based on the group values from the recent publications [34,35].

3.1. H-atom abstraction reactions

H-atom abstraction reactions from the DIB isomers are dominated by abstractions from the allylic sites due to the combination of the relatively weaker allylic C–H bonds and their high degeneracy. DIB-1 has five allylic hydrogen atoms and nine primary hydrogen atoms, whereas DIB-2 has six allylic hydrogen atoms and nine primary hydrogen atoms. H-atom abstractions from an allylic carbon atom are the most facile at low temperatures due to their relatively low C–H bond energy. Abstraction from alkyl sites are the next important abstraction reactions followed by the abstraction of vinylic hydrogen atoms. The analogous propene/isobutene rate parameters were used for primary allylic H-atom abstraction by $\dot{\text{O}}$, $\dot{\text{O}}\text{H}$ and $\text{H}\dot{\text{O}}_2$ radicals, and O₂ from various studies [18,36–38]. To simulate H-atom abstraction reactions from the secondary allylic site, respective 1-butene (C₄H₈-1) analogies were used [37,39,40]. The rate constants for abstraction of the primary hydrogens were adapted by analogy with iso-octane kinetics [41,42], assuming that the presence of the C=C double bond has no influence, given its distance from these atoms. The abstractions from the vinylic sites have been modeled using analogies with the C₁–C₄ core mechanism.

3.2. Intra-molecular H-atom shifts of DIB radicals

Allylic and alkylic DIB radicals formed from H-atom abstraction reactions can interconvert through intramolecular H-atom shift reactions, which occur during alkene pyrolysis and oxidation. In the

current model, high-pressure rate constants of intramolecular H-atom shift reactions of both alkyl and allylic radicals were adapted from a recent theoretical investigation by Wang et al. [43] using electronic structure calculations at the CBS-QB3 level of theory.

3.3. Radical addition to molecular oxygen

The addition of allylic fuel radicals to O₂ is less facile than for their non-allylic radical [44–46] counterparts. However, the chemistry subsequent to allylic radical addition to O₂ has been shown to be important in accurately predicting the ignition propensity of isobutene [18]. For this reason, the addition of allylic DIB radicals to O₂ molecules leading to the formation of alkenyl-peroxy radicals are included in the mechanism, and have been modeled by analogy with isobutene from Chen and Bozzelli [47]. The reactions including intramolecular H-atom shift reactions to form hydro-peroxy alkyl radicals ($\dot{\text{Q}}\text{OOH}$) and the second radical addition reactions to O₂ are adapted from Chen and Bozzelli. For addition of alkylic DIB radicals to O₂, alkylic radicals on the methyl groups attached to the quaternary carbon can readily add to O₂ at low temperatures forming alkyl peroxy radicals. The alkyl peroxy radicals are similar to their counterparts in alkanes and can eventually produce carbonyl-hydroperoxides and $\dot{\text{O}}\text{H}$ radicals through a series of internal H-atom isomerizations and radical addition to O₂ reactions. This reaction sequence is expected to contribute to the low temperature reactivity of the DIB isomers, and the relevant reaction rate coefficients were derived from reaction rate rules developed for alkanes [48].

3.4. Cyclo-addition reactions of alkenyl-peroxy radicals

The present mechanism describes the formation of cyclo-peroxy alkyl radicals produced from intramolecular cyclo-addition reactions of the peroxy group onto the double bond. This class of reactions, which was rarely modeled in earlier literature mechanisms, was found to be important in the recent kinetic modeling of isobutene and the linear pentene isomers. Therefore, for completeness in the model, these reactions are included using the rate constants from a recent high-level calculation from Sun et al. [49].

3.5. Reactions of allylic and $\text{H}\dot{\text{O}}_2$ radicals

Previous studies [44,50,51] have concluded that allylic radicals react with $\text{H}\dot{\text{O}}_2$ radicals and decompose or undergo chemically activated channels to produce alkenoxy and hydroxyl radicals. These reactions convert less reactive $\text{H}\dot{\text{O}}_2$ radicals into reactive $\dot{\text{O}}\text{H}$ radicals, promoting reactivity at low and intermediate temperatures. The kinetic model developed in this work has adopted the pathway of recombination followed by decomposition to allyloxy radical + $\dot{\text{O}}\text{H}$, and the chemically activated pathway, with the reaction rates taken by analogy with propene oxidation kinetics [50].

3.6. Radical addition to the double bond

3.6.1. $\dot{\text{O}}\text{H}$ radical addition

In the low-to-intermediate temperature regime, the presence of the C=C double bond can enable an $\dot{\text{O}}\text{H}$ radical addition pathway, producing alcoholic radicals that can then add to O₂ to form hydroxy alkyl-peroxy (HAP) radicals. The HAP radicals so formed can react via the Waddington mechanism, which involves an internal H-atom transfer from the hydroxyl site, followed by decomposition into two aldehyde molecules and one $\dot{\text{O}}\text{H}$ radical. However, the hydrogen atom may also be transferred from a carbon atom rather than from the –OH group, which is similar to a typical $\text{R}\dot{\text{O}}_2$ isomerization reaction in the low temperature oxidation of alkanes. In this way, the addition of $\dot{\text{O}}\text{H}$ radicals to the double bond in an

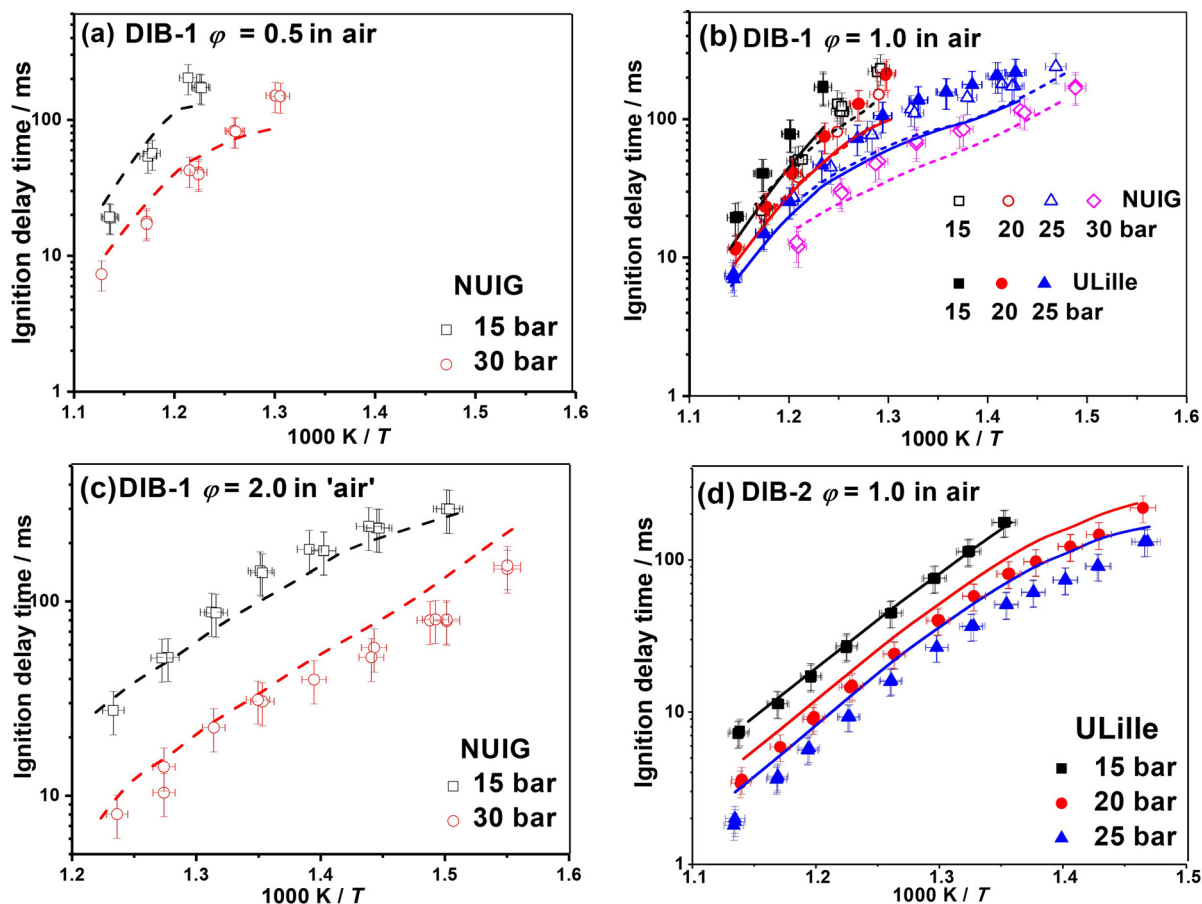


Fig. 4. The current model predictions for DIB isomers; IDTs measured at NUIG and ULille RCM at (a) DIB-1 $\phi = 0.5$, (b) DIB-1 $\phi = 1.0$, (c) DIB-1 $\phi = 2.0$ and (d) DIB-2 $\phi = 1.0$ at pressures ranging from 15 – 30 bar. Open and solid symbols correspond to NUIG and ULille experimental data respectively. Dashed and solid lines correspond to IDT predictions using RCM volume histories from NUIG and ULille respectively.

alkene can initiate alkane-like low temperature reaction pathways [48]. In assigning the associated rate constants to these pathways, OH addition to the C=C double bond was taken by analogy with OH addition to propene from [52] with a branching ratio of 75:25, favoring addition to the terminal carbon atom. Rate constant expressions for the next steps of radical additions to O₂, internal isomerization, dissociation reactions, and alternate Waddington pathways were modeled using analogous rate constants to those published by Sun et al. [53].

3.6.2. HO₂ radical addition

HO₂ radical concentrations are relatively high at intermediate temperatures (750 – 1000 K) [37], and these can recombine with allylic radicals or add on to the double bond forming hydroperoxy alkyl radicals. To describe HO₂ radical additions to the double bond, analogies to ethylene and isobutene rate constants were taken from the calculations by Zádor et al. [37] for internal and terminal additions, respectively.

3.6.3. H atom addition

H-atom addition to the C=C double bond in the DIB isomers forming iso-octane radicals was modeled as the decomposition of iso-octane radicals adopting the analogous rate constants from Wang et al. [54].

4. Results and discussion

IDTs for DIB isomers were measured in both RCMs at pressures and temperatures relevant to practical applications, i.e., 15

– 30 bar and 650 – 900 K at equivalence ratios in the range of 0.5 – 2.0. IDTs of both isomers were measured in the ULille RCM while the NUIG experiments focused on the DIB-1 isomer only. To ensure fidelity and consistency in the measurements, experiments were conducted at similar conditions for the stoichiometric DIB-1/oxidizer mixtures at compressed pressures of 15 bar, 20 bar and 25 bar. As seen in Fig. 4(b), the experimental measurements at 20 bar and 25 bar from the two different facilities compare well, and the differences are within the experimental uncertainty (25%). However, the measurements at 15 bar show larger differences. Experiments were repeated at both the facilities to resolve the differences at this condition, but the measurements were found to be highly repeatable using both facilities, and the differences unfortunately could not be explained. For other experimental observations, the lack of classical negative temperature coefficient (NTC) behavior in the temperature range investigated is noted. The IDTs did exhibit a non-Arrhenius behaviour which can be seen in Fig. 4(a) – 4(d). Furthermore, we did not notice two-stage ignition for both isomers over the temperature range investigated herein. This lack of two stage ignition can be seen in pressure traces shown in Fig. 3.

The model can reproduce the IDT experiments from the two different RCM facilities well; Fig. 4(b) represents common experiments (for DIB-1) and simulations using the corresponding heat loss profiles. In Fig. 4(b), the solid and open symbols represent the IDT experiments using the ULille RCM and NUIG RCM, respectively. Simulations were performed including the corresponding heat loss profiles i.e., solid and dashed lines represent the ULille and NUIG data, respectively. However, the model is faster (~25%) than

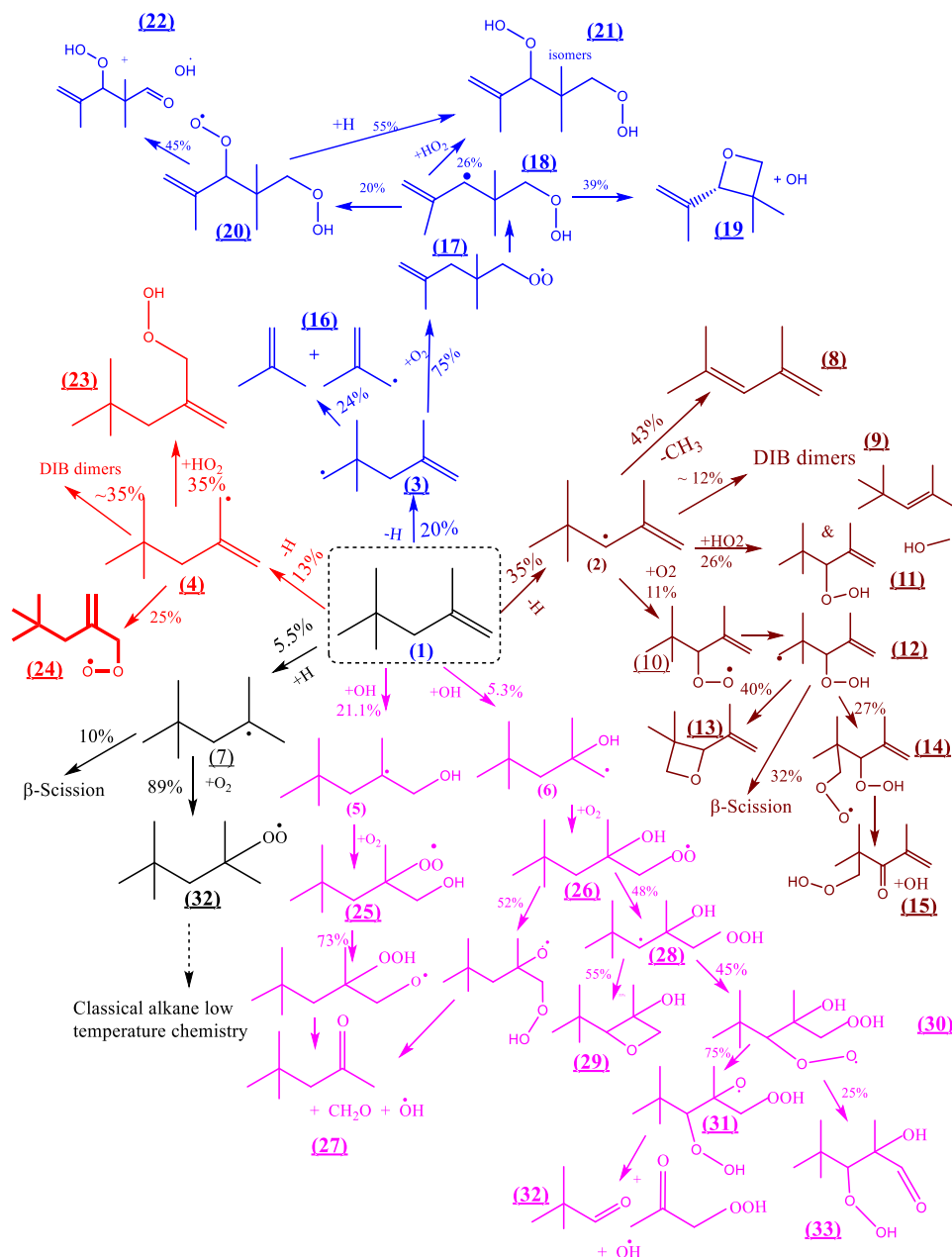


Fig. 5. Flux analysis using the current model for DIB-1 oxidation at $\varphi = 1.0$ in air, 25 bar at 700 K at the time of 20% fuel consumption.

the experiments in the temperature range of 715 – 770 K at all pressures. Further comparisons and discussion on the relative reactivity of the two isomers shall be presented in later sections.

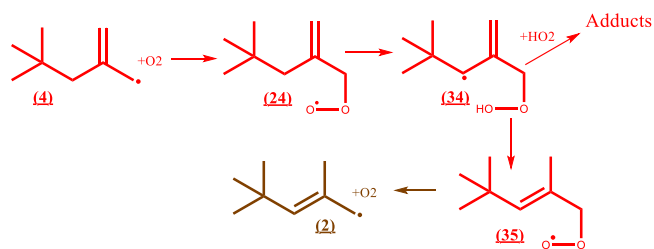
Fig. 5 depicts the main reaction pathways of DIB-1 (1) at the $\varphi = 1.0$, 700 K, 25 bar condition at the time of 20% fuel conversion. In total, 73% of DIB-1 undergoes H-atom abstraction reactions, of which 35%, 20%, and 13% forms secondary allylic (2), alkyl (3), and primary allylic (4) radicals, respectively. Radical addition reactions to the C=C double bond are responsible for approximately 31.5% of fuel consumption, of which 26.4% comes from OH radical addition (5) and (6), with 5.5% occurring via H atom addition (7). IC8D3-5R (2) allylic radicals, produced via abstraction of secondary-allylic hydrogen atoms, are largely consumed via β -scission reactions and radical + radical reactions. The β -scission reactions produce 2,4-dimethyl-1,3-butadiene (8) and methyl radicals. The other important reactions of IC8D3-5R include reactions with HO₂ radicals producing olefinic hydroperoxide adducts: IC8D3-5OOH, IC8D4-3OOH (10) in addition to the chain-terminating self-recombination

reactions producing C₁₆ adducts (DIB dimers) (9). The latter two reactions are analogous to the reactions of allyl (\dot{C}_3H_5 -a) and methyl-allyl (\dot{C}_4H_7) radicals. Addition to molecular oxygen producing the secondary allylic-peroxy radical, IC8D4-3O₂ (11) is another reaction channel consuming IC8D3-5R radicals (2).

4.1. DIB-1 kinetic analyses

The secondary allylic peroxy adduct undergoes internal isomerization reaction via a H-atom isomerization from methyl substitutions on the tert-butyl group resulting in the production of a QOOH-like radical with alkyl characteristics, namely IC8D4OOH3-1R (12).

This radical is subsequently consumed by unimolecular reactions and addition to molecular oxygen, with the former reaction class dominating its consumption. These unimolecular reactions produce an unsaturated cyclic ether (13) together with an OH radical. The addition of IC8D4OOH3-1R (12) to O₂ facilitates the



Scheme 1. Chemistry of IC8D4-5O2R radicals.

formation of IC8D4Q3-1O₂ (**14**), which is a \dot{O}_2 QOOH-like species which subsequently produces IC8DQ1Y3 (**15**), an olefinic keto-hydroperoxide and an $\dot{O}H$ radical.

H-atom abstraction from the tert-butyl group are the next important reactions producing IC8D4-1R (**3**) radicals which are alkylic in nature. The important reactions controlling IC8D4-1R (**3**) consumption are addition to molecular oxygen (75%) leading to the peroxy adduct species IC8D4-1O₂R (**17**). Moreover, IC8D4-1R (**3**) is consumed (25%) by β -scission reactions producing isobutene and methyl allyl (iC_4H_7) radicals (**16**). The peroxy adducts undergo internal H-atom isomerization reactions producing IC8D4OOH1-3R (**18**), which are resonance stabilized QOOH radicals. These radicals are consumed by unimolecular and bimolecular reactions. The unimolecular reactions form an unsaturated cyclic ether (**19**) and an $\dot{O}H$ radical; this reaction is similar to the formation of a cyclic ether and an $\dot{O}H$ radical from QOOH radicals in alkanes. The bimolecular reactions of IC8D4OOH1-3R (**18**) radicals include reactions with O₂ and HO₂ radicals. Reactions of IC8D4OOH1-3R (**18**) with O₂ produce IC8D4OOH1-3O₂ (**20**), \dot{O}_2 QOOH like radicals) while reactions with HO₂ produce dihydroperoxy adducts IC8D4Q13 (**21**), IC8D3Q15 (not shown, an isomer of **21**), respectively. IC8D4OOH1-3O₂ (**20**) radicals isomerize to produce keto-hydroperoxide-like species IC8D4Q3Y1 (**22**). IC8D4OOH1-3O₂ (**20**) radicals also participate in termination reactions to produce IC8D4Q13, IC8D3Q15 (not shown, an isomer of **21**). The low-temperature chemistry of IC8D4-1R (**3**) may produce the following hydroperoxides: IC8D4Q13 (**21**), IC8D4Q3Y1 (**22**), IC8D3Q15 (not shown, an isomer of **21**), which upon decomposition generate $\dot{O}H$ radicals; a process which facilitate chain branching at low temperatures.

H-atom abstraction from the primary allylic sites produce IC8D4-5R radicals (**4**). The consumption of these radicals is largely similar to that for IC8D3-5R (**2**) radicals, and the main reaction channels are addition to molecular oxygen, self-recombination reactions, and adduct formation with HO₂ radicals. The self-recombination reactions produce DIB-dimers (**8**), while reactions with HO₂ radicals produce the hydroperoxy adduct, IC8D4-5OOH (**23**). The addition of IC8D4-5R to O₂ leads to the production of the peroxy adduct: IC8D4-5O2R (**24**) which undergo unimolecular isomerization reactions via a H-shift of a secondary allylic hydrogen atom to produce IC8D4Q5-3R (**34**) radicals, which are QOOH-like radicals. This isomerization reaction is similar to that observed in the oxidation of isobutene in our earlier work [18]. IC8D4Q5-3R (**34**) radicals are consumed by reactions with O₂, HO₂ producing peroxy- and hydroperoxide adducts but an additional interesting reaction network as shown below is found to be important, resulting in the conversion of IC8D4-5R radicals to IC8D3-5R radicals. **Scheme 1**

The addition of $\dot{O}H$ radicals and \dot{H} atoms to the double bonds in DIB-1 leads to the formation of alcohol (**5**) and (**6**) and alkyl (**7**) radicals, respectively. The alcohol radicals are consumed by Waddington pathways which involve addition to O₂ followed by H-shifts from the -OH moiety to the peroxy site producing alkoxy-

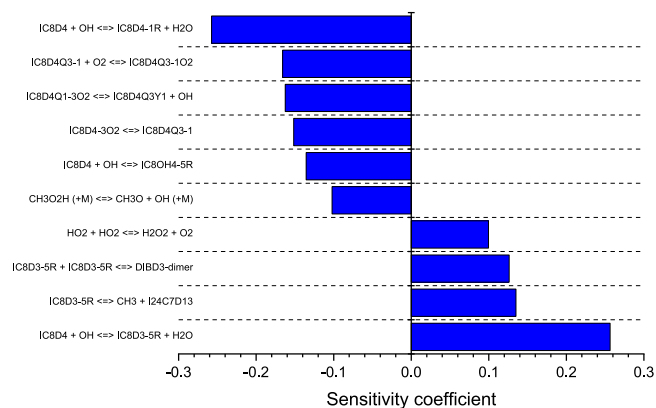


Fig. 6. Brute force sensitivity analysis representing reactions controlling DIB-1 IDTs using the new model at $\phi = 1.0$ in air, $p_c = 25$ bar, and $T_c = 700$ K.

hydroperoxides which decompose to produce aldehydes/ketones and $\dot{O}H$ radicals. The Waddington pathways largely result in chain propagation reactions, but in the present analysis we do observe that the addition of $\dot{O}H$ to the internal sp^2 carbon results in chain branching pathways downstream. IC8O4H-5O₂R (**26**), peroxy adducts of IC8O4H-5R (**6**) participate in $\dot{R}O_2 = \dot{Q}OOH$ type reactions involving the H-atoms on secondary carbons in the chain producing IC8O4H4Q5-3R (**28**) radicals. This reaction which is often characterized as an alternative-Waddington pathway and is competitive due to the facile 6-member transition state resulting in a relatively low activation energy barrier for reaction. The alcoholic-hydroperoxy alkyl radical IC8O4H4Q5-3R (**28**) is subsequently consumed via a second addition to O₂ and unimolecular elimination reactions to produce a hydroxy cyclic-ether (**29**). The peroxy adduct IC8O4H4Q5-3RO₂ (**30**), produced via addition to O₂ in (**28**) can be consumed by H-shifts from the OH moiety in (**31**) or by the formation of an alcohol-ketohydroperoxide IC8O4H4KET53 (**33**) through H-isomerization from the -COOH site. Formation of (**30**), and its subsequent reaction producing (**32**) and (**33**) facilitate chain branching at low temperatures. However, the fluxes through the formation of these intermediates are lower compared to the chain propagating pathways which produce (**27**) and (**29**).

Fig. 6 presents the top 10 most sensitive reactions influencing IDTs at 700 K. It can be inferred that reactions producing and consuming IC8D3-5R (**2**) radicals inhibit reactivity while those producing and consuming IC8D4-1R (**3**) radicals and addition of $\dot{O}H$ radicals to the double bond promote reactivity. The reactions of (**2**) which inhibit reactivity are: IC8D4 (**1**) + $\dot{O}H \rightarrow$ IC8D3-5R (**2**) + H₂O, IC8D3-5R (**2**) \rightarrow I24C7D13 (**9**) + $\dot{C}H_3$, IC8D3-5R (**2**) + IC8D3-5R (**2**) \rightarrow DIB3-DIMER (**10**). This inhibiting effect on reactivity in forming IC8D3-5R (**2**) radicals is due to their lack of chain branching reactions. As shown in **Fig. 5**, IC8D3-5R (**2**) radicals are primarily consumed by β -scission reactions producing a diene (**9**) intermediate in addition to methyl radicals. The reaction network of IC8D3-5R (**2**) radicals, which starts with H-atom abstraction by reactive $\dot{O}H$ radicals results in the formation of methyl radicals which are less reactive than $\dot{O}H$ radicals. Thus, this network inhibits reactivity. The self-recombination reactions producing DIB dimers (**10**) also result in radical scavenging. The reactions of IC8D3-5R (**2**) radicals with HO₂ radicals forming hydroperoxide adducts (**11**) can facilitate chain propagation, but the decomposition of the hydroperoxide adducts to $\dot{O}H$ radicals have relatively high activation energy barriers (~ 43 kcal mol⁻¹). The abstractions from the tert-butyl group producing IC8D4-1R radicals promotes reactivity as the chemistry downstream initiated by this radical can facilitate chain branching chemistry through the reaction sequence IC8D4-

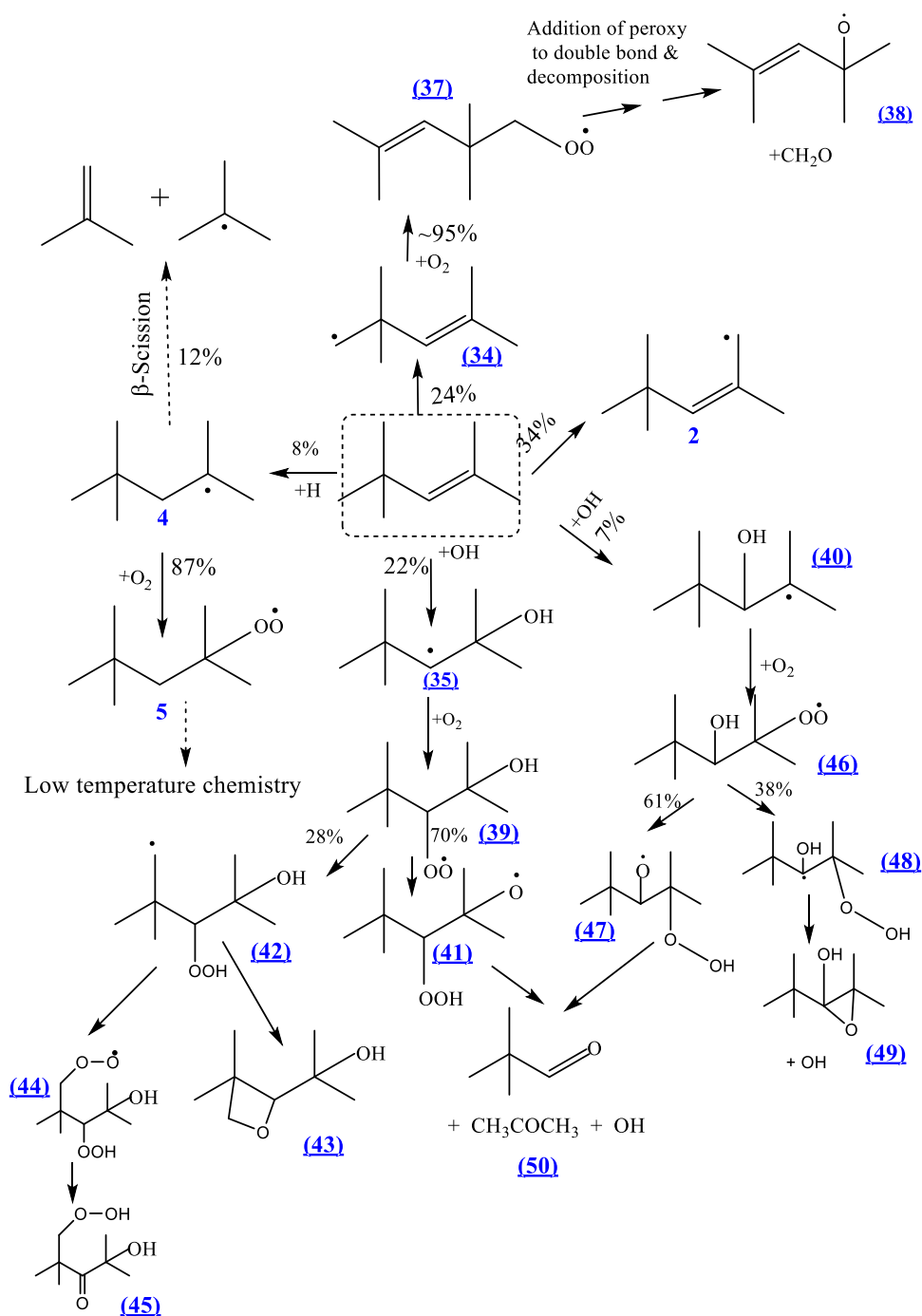


Fig. 7. Flux analysis using the current model for DIB-2 oxidation at $\phi = 1.0$ in air, 30 bar at 700 K, and 20% fuel consumption.

1R (**3**) + O₂ → IC8D4-1O₂R (**17**), IC8D4-1O₂R (**17**) → IC8D4OOH1-3R (**18**), IC8D4OOH1-3R (**18**) + O₂ → IC8D4OOH1-3O₂R (**20**) and IC8D4OOH1-3O₂R (**20**) → IC8D4Q3Y1 (**22**) + OH. The reaction IC8D4 (**1**) + OH → IC8OH4-5R (**6**) promotes reactivity as the chemistry of IC8OH4-5R radicals downstream can facilitate chain branching via the formation of (**33**).

4.2. DIB-2 kinetic analyses

The flux analysis using the current model for DIB-2 oxidation at $\phi = 1.0$, 25 bar and 700 K, at 20% fuel consumed is depicted in Fig. 7. The DIB-2 isomer is mainly consumed via H-atom abstrac-

tion reactions at the primary allylic (34%) and alkylic (24%) sites, forming radicals (**2**) and (**34**) respectively. The H-atom abstraction reactions from the primary allylic site produces IC8D3-5R (**2**) radical and the consumption chemistry of this radical is similar to that shown in Fig. 5 and shall not be discussed again. H-atom abstraction reactions from the methyl sites on the tert-butyl group leads to the production of primary alkyl radicals, IC8D3-1R (**34**), which are consumed primarily by addition to O₂. The peroxy adducts so formed, IC8D3-1O₂R (**37**) undergo intramolecular additions on the double bonds producing cyclic peroxy adducts. The cyclic peroxy adducts eventually undergo unimolecular decomposition producing formaldehyde and olefinic alkoxy radicals (**38**). The rest

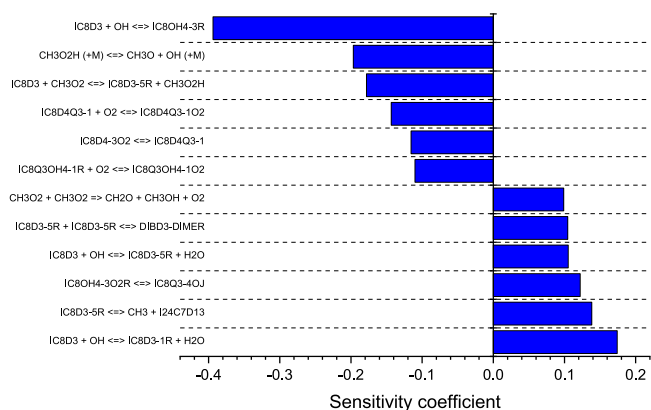


Fig. 8. Brute force sensitivity analysis representing reactions controlling DIB-2 IDTs using the new model at $\varphi = 1.0$ in air, $p_C = 25$ bar, and $T_C = 700$ K.

of the DIB-2 flux is consumed via addition reactions, 8% via H atom addition at the secondary vinylic position with the double methyl substitution, forming iC_8-4R (7) radicals. These undergoes β -scission (56%), producing iC_4H_8 and tC_4H_9 , while the remaining 44% undergoes O_2 addition (5) and classical low temperature chain branching kinetics.

$\dot{O}H$ radical addition reactions to the C=C bond account for 22% and 7% of DIB-2 flux, forming hydroxy alkyl radicals IC8OH4-3R (35) and IC8OH3-4R (40) radicals from the addition of $\dot{O}H$ radicals to tertiary and secondary carbon atoms, respectively. These hydroxy alkyl radicals react with O_2 undergoing the conventional and alternative Waddington pathways. The Waddington pathways are the major consumption pathways, producing intermediates (41) and (46), accounting for more than 60% of the flux. The classical Waddington pathways produce acetone, 2,2-dimethyl propanal and $\dot{O}H$ (50). The alternative-Waddington pathways account for up to 40% of the consumption flux. The main products of the alternative-Waddington pathways are alcohol-substituted cyclic ethers ((43) and (49)), and largely lead to chain propagation reactions producing $\dot{O}H$ radicals. The alternative Waddington pathways initiated by $\dot{O}H$ radical additions to the tertiary carbon could lead to chain branching through the reaction sequence: IC8Q3OH4-1R (42) + $O_2 \rightarrow$ IC8Q3OH4-1 \dot{O}_2 (44), IC8Q3OH4-1 \dot{O}_2 (44) \rightarrow IC8OH4KET31 (45) + $\dot{O}H$. The $\dot{O}H$ additions to the secondary carbon in DIB2 producing IC8OH3-4R (40) radicals largely leads to the formation of (50) and (49) which do not facilitate chain branching. Thus, the selectivity of $\dot{O}H$ addition to double bond can have implications on the reactivity of DIB2.

The most sensitive reaction which promotes reactivity of DIB-2 is the addition of $\dot{O}H$ to the double bond producing IC8OH4-3R (35). As mentioned earlier, this reaction can promote chain branching at low temperatures through the alternative Waddington pathways. It is for the same reason that the formation of HAP (IC8Q3OH4-1R (42) + $O_2 \rightarrow$ IC8Q3OH4-1 \dot{O}_2 (44)) also appears in the list of the top sensitive reactions promoting reactivity and the competitive classical Waddington pathway channel IC8OH4-3 $\dot{O}_2R \rightarrow$ IC8Q3-4 $\dot{O}J$ appears as a sensitive reaction retarding ignition. H-atom abstraction by $\dot{O}H$ radicals from the allylic and the methyl sites on the *ter*-butyl part of the molecule retard ignition as they compete with addition of $\dot{O}H$ to double bond producing IC8OH4-3R (35), and ignition is also retarded as the resulting radicals do not effectively lead to chain branching. The IC8D3-5R radicals produced from H-atom abstraction from the allylic sites largely participate either in chain terminating reactions producing DIB dimers or undergo methyl-eliminations producing dimethyl-pentadienes. The peroxy adducts of IC8D3-5R (Fig. 8) could participate in some chain branching chemistry through

Table 4

Flux (%) of fuel through addition and abstraction reactions.

Reaction type	DIB-1	DIB-2
H-atom abstraction	69.5	59.37
Addition to the double bond	28.5	39.31
$\dot{O}H$ addition	15.64	17.07
$H\dot{O}_2$ addition	1.08	9.30
H addition	9.66	11.00
H-addition (Chemically activated pathways)	1.64	1.42
\dot{O} -addition (Chemically activated pathways)	0.48	0.52

the reaction sequence: IC8D4-3 $\dot{O}_2 \rightarrow$ IC8D4Q3-1 \rightarrow IC8D4Q3-1 + $O_2 \rightarrow$ IC8D4Q3-1 \dot{O}_2 which explains their presence in the list of sensitive reactions. It is interesting to note that abstractions from methyl-peroxy producing methyl hydroperoxide and the decomposition of methyl hydroperoxide appear to promote reactivity. This is because abstraction reactions by methyl peroxy radicals compete with H-atom abstractions by $\dot{O}H$, and the resulting methyl-hydroperoxide molecules decompose to produce $\dot{O}H$ radicals. The methyl peroxy radicals can also participate in self-recombination reactions $CH_3\dot{O}_2 + CH_3\dot{O}_2 \rightarrow CH_2O + CH_3OH + O_2$ which are chain terminating in nature. These chain terminating reactions also lowers the flux through H-atom abstractions reactions, thus retarding reactivity.

4.3. Reactivity comparison of DIB isomers

Reactivity comparisons using the experimental IDTs (ULille) of stoichiometric ($\varphi = 1.0$) DIB-1 and DIB-2 in air mixtures at 15, 20, and 25 bar are presented in Fig. 9(a) – 9(c). In the investigated p_C/T_C conditions, DIB-2 exhibits faster reactivity (lower IDTs) compared to DIB-1.

The position of the double bond in the DIB isomers, therefore, influences the reactivity. The influence of the position of the double bond could be due to differences in relative fluxes through reactions of reactive radicals (H, $\dot{O}H$, $H\dot{O}_2$) through abstraction and additions reactions. To gain insights into the chemistry controlling the reactivity of the isomers, a flux analysis was conducted at a compressed temperature of 800 K and at a pressure of 20 bar. This condition was chosen as the relative reactivity of the isomers was captured well by the mechanism for the different pressures considered. The flux analysis was conducted at 20% fuel conversion and the summary of the flux through the abstractions and additions reaction is shown in Table 4.

From the flux analysis we see that the percentage flux through the abstraction reactions for the DIB-1 isomer is higher compared to DIB-2 by about 10%, while the fluxes through addition reactions to the double bond are higher in the case of DIB-2 by a similar margin. The biggest difference in the percentage flux through additions appears to stem from the difference in the flux through $H\dot{O}_2$ radical additions. These additions are modeled using kinetic analogies to reactions of $H\dot{O}_2$ with ethylene, propene, iso-butene and the linear butene isomers published by Zádor et al. [37]. The $H\dot{O}_2$ radical additions to the double bond may result in the formation of oxiranes + $\dot{O}H$ either through chemically activated pathways or via the formation of $\dot{Q}OOH$ iso-octane radicals. These addition reactions facilitate an efficient conversion of $H\dot{O}_2$ into $\dot{O}H$ radicals. The flux through addition of $\dot{O}H$ radicals and H atoms to the double bond in the DIB-2 isomer are higher too, but the differences are smaller compared to those for $H\dot{O}_2$ radical additions. Thus, based on the present flux analysis, the higher reactivity of DIB-2 can be attributed to sensitivity of the addition reactions to the location of the double bond, and in particular the site-specific addition of $H\dot{O}_2$ radicals.

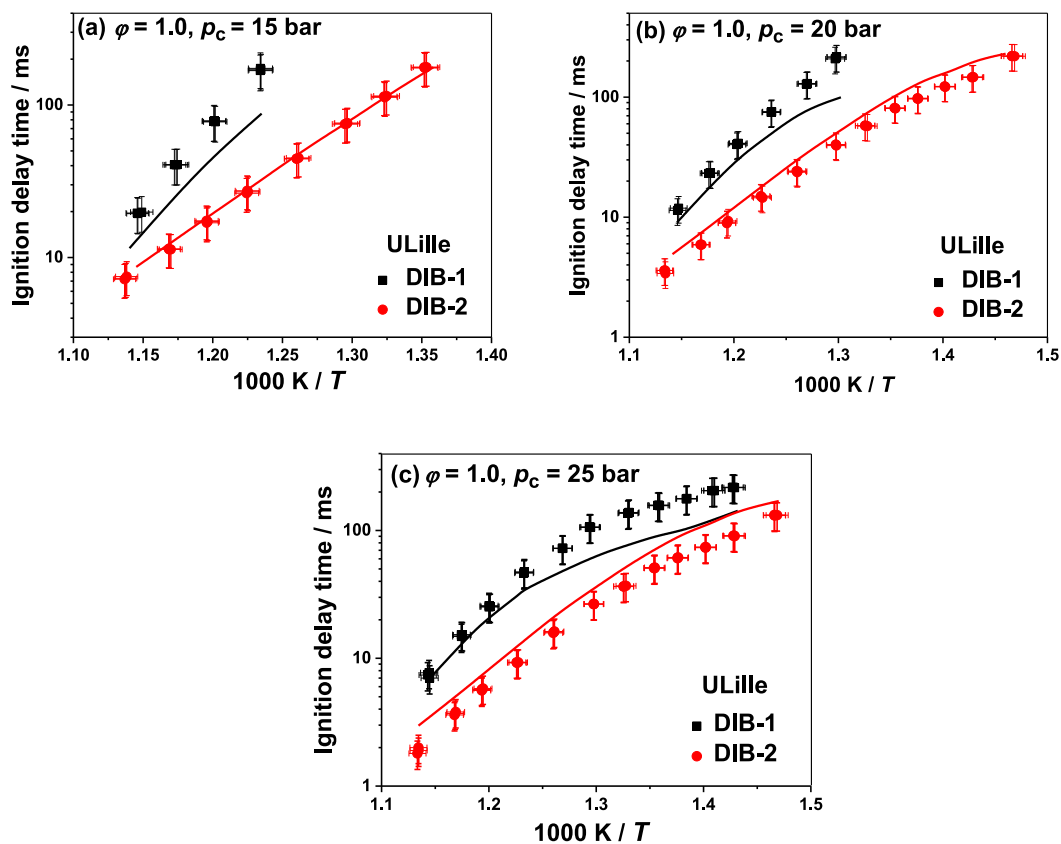


Fig. 9. The current model predictions for DIB isomers; IDTs measured at ULille RCM at $\phi = 1.0$ fuel in air at (a) 15, (b) 20 and (c) 25 bar.

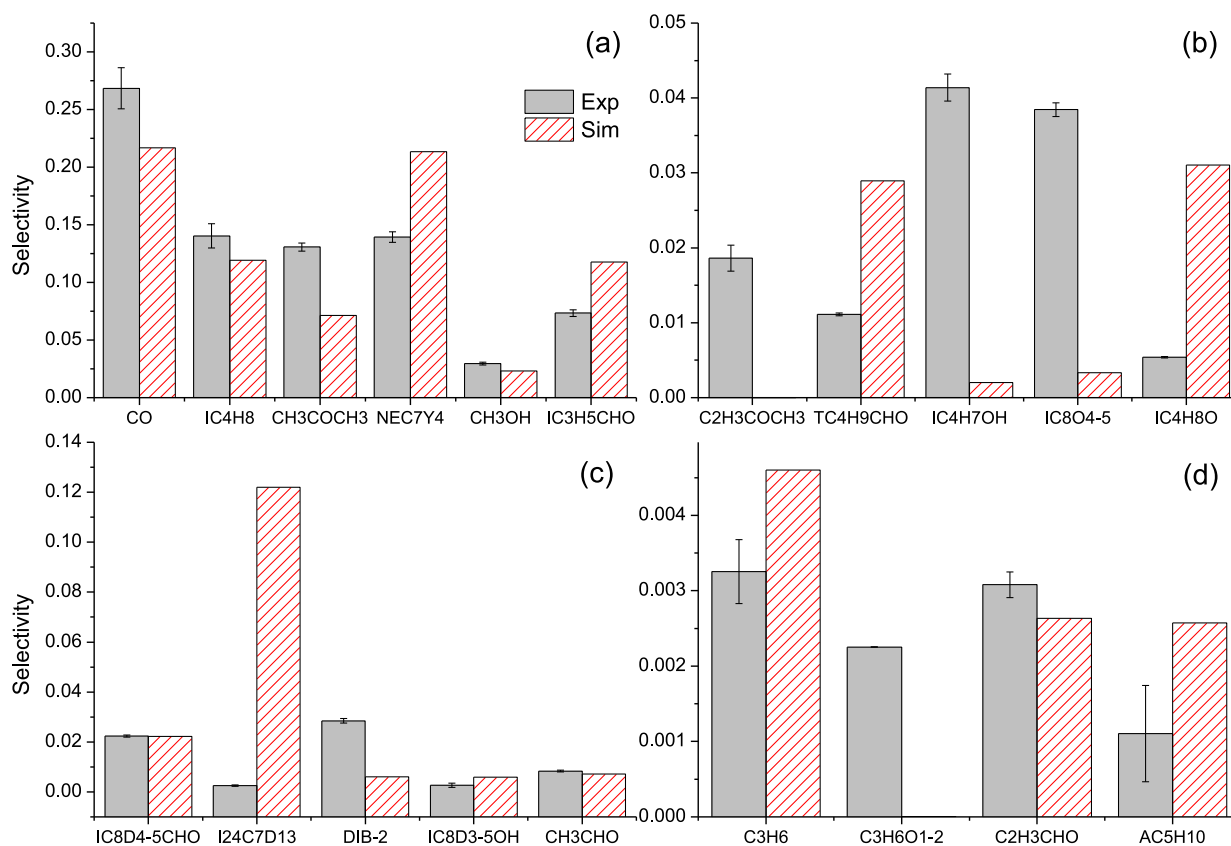


Fig. 10. RCM species selectivity for DIB-1 at $T_c = 700$ K, $P_c = 25$ bar, $\phi = 1.0$ in air. For clarity of species nomenclature, please refer to the dictionary provided in the supplemental material.

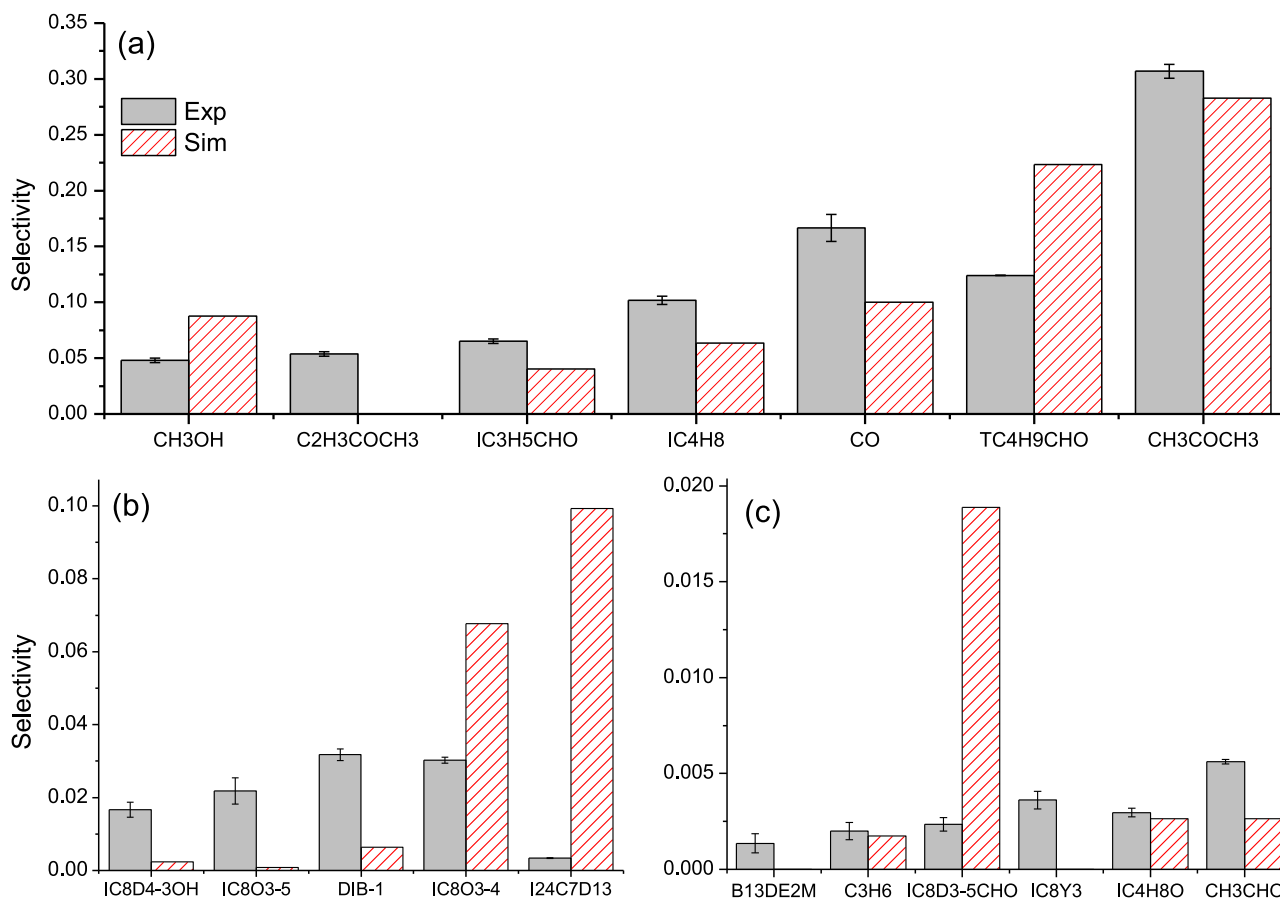


Fig. 11. RCM species selectivity for DIB-2 at $T_c = 700$ K, $P_c = 25$ bar, $\phi = 1.0$ in air. For clarity of species nomenclature, please refer to the dictionary provided in the supplemental material.

4.4. Speciation data

Speciation measurements were conducted in RCM and CNRS-JSR to provide information on the formation of intermediates during fuel oxidation. These measurements are expected to provide an additional rigor in the validation of the mechanism and ensure that it successfully captures the oxidation chemistry. In this section, we show and discuss the predictive fidelity of the mechanism in capturing the measured speciation measurements.

4.4.1. RCM Speciation data

To better understand the low temperature kinetics, sampling experiments in the ULille RCM for neat DIB-1 and DIB-2 were performed to identify and quantify the stable intermediate species formed during the ignition delay period, at $T_c = 700$ K, $p_c = 25$ bar, and $\phi = 1.0$. All samples from the reacting mixture were extracted from the reaction chamber and immediately expanded into a previously evacuated and heated sampling canister to quench the reactivity (please refer to Section 2.2 for further details) and analysed using two GCs. Intermediates with a mole fraction higher than 50 ppm were used to validate the current model. Most of the experimentally observed intermediates correspond well with the DIB-1 model simulations as shown in Fig. 10. The decomposition reactions of DIB-1 result in large quantities of isobutene (iC_4H_8) [18] which is slightly under-predicted ($\sim 15\%$) by the current model, while meeting the estimated experimental uncertainties of $\pm 15\%$. OH radical addition to the terminal vinylic site of DIB-1 and subsequent Waddington mechanism results in the production of 4,4-dimethyl-2-pentanone (neC_7Y_4) and formaldehyde (CH_2O). CH_2O was observed in the MS chromatograms but

was not quantified. NEC_7Y_4 , one of the Waddington products, is over-predicted by $\sim 50\%$.

In the case of DIB-2, at 700 K, conversion primarily proceeds via the Waddington mechanism and results in the production of tC_4H_9CHO and acetone. The current model reproduces the measured acetone profile well and is within a factor of two of the experimental tC_4H_9CHO profile. In addition, other stable species in the model, such as CH_3OH , C_3H_6 , CH_3CHO , iC_4H_8 , $a-C_5H_{10}$, methylacrolein, etc., are well reproduced. However, the current model is consistently less accurate for the oxiranes and oxetanes produced during DIB oxidation; for instance 2-methyl-2-neopentyl-oxirane (iC_8O4-5) for DIB-1 and 2-tert-butyl-3,3-dimethyl oxirane (iC_8O3-4) for DIB-2. Considering that the addition of HO_2 to the double bond is important in capturing the relative reactivity of the isomers, high-level theoretical calculations on the reaction rate constants for fuel addition reactions with HO_2 for larger iso-olefins are recommended for future work.

4.4.2. JSR Speciation data

Figures 11–13 represent the validation of the DIB model developed in this study against the stable species profiles measured in the ICARE Orléans JSR for the oxidation of DIB-1 and the DIB-1/DIB-2 mixtures respectively. The experiments were conducted at 10 atm over a temperature range 720 – 1200 K, at $\phi = 1.0$ with an initial fuel mole fraction of 1000 ppm. The model is in adequate agreement with most of the species over a wide range of experimental conditions as shown in Figs. 12 and 13 ($\phi = 1.0$ and 10 atm). Additional validation plots ($\phi = 0.5$ and 2.0 at 10 atm) of DIB-1 and the mixture (DIB-1 and DIB-2) are included as Supplementary material.

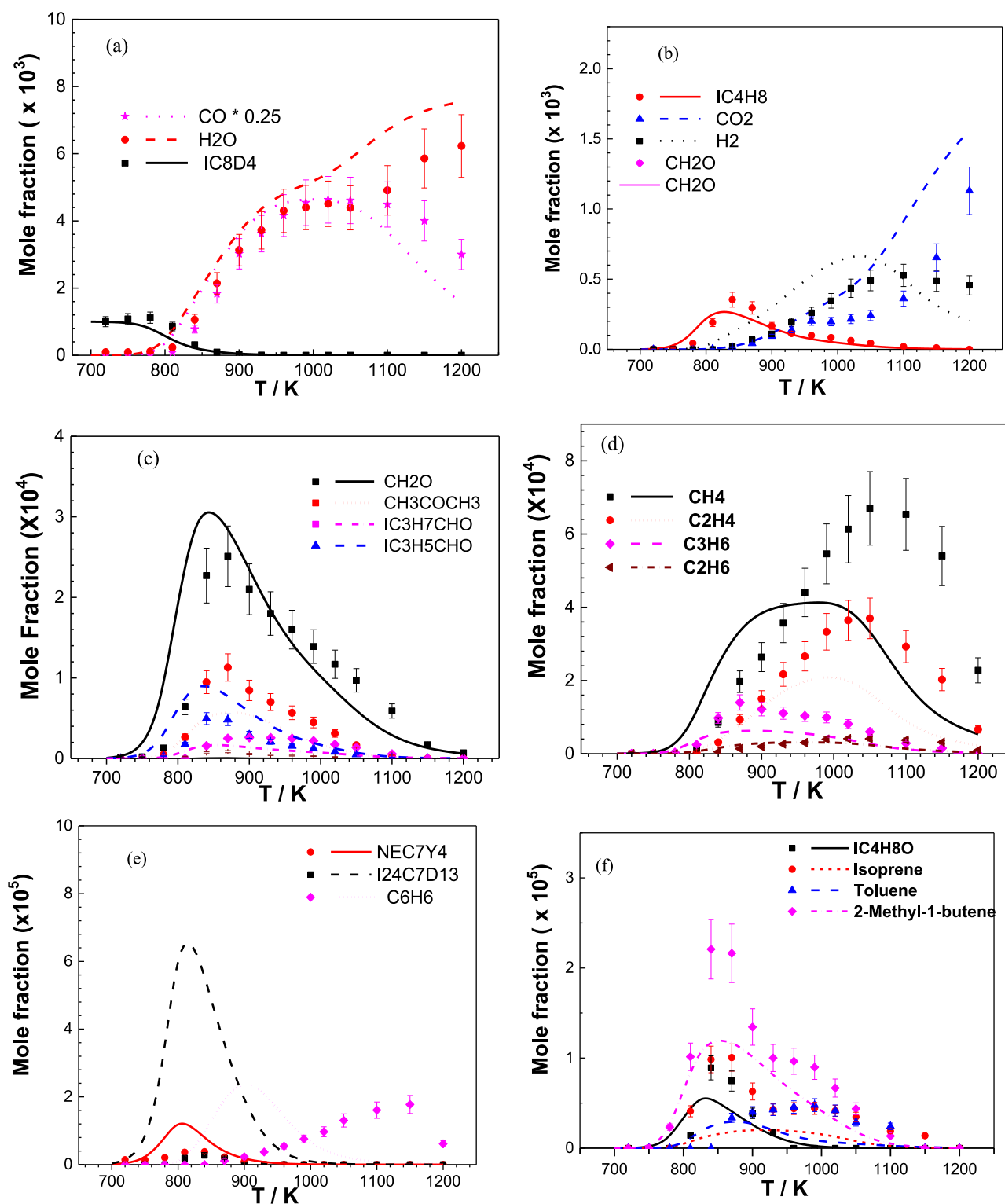


Fig. 12. Neat DIB-1 oxidation species profiles for 1000 ppm DIB-1 and $\phi = 1.0$, at $p = 10$ atm and $\tau = 0.7$ s in the JSR. Points are new experimental results, and lines represent current DIB model simulations. For clarity of species nomenclature, please refer to the dictionary provided in the supplemental material.

Conversion of the neat DIB-1 and DIB-2 mixtures starts at ≈ 800 K and ≈ 780 K, respectively, at all equivalence ratios. A higher reactivity is observed in both experiments and simulation as the mixtures get leaner at a given temperature, Fig. 12(a), Fig. 13(a), Fig. S1(a), Fig. S2(a) and Fig. S3(a). In these JSR experiments, $[X_{O_2}]$ increases as the mixtures get leaner while the $[X_{Fuel}]$ is unchanged. Higher $[X_{O_2}]$ is expected to increase the efficacy of the

low temperature pathways which explains the higher reactivity of the leaner mixtures.

5. Uncertainties in DIB chemistry and modeling needs

From the comparison of simulated speciation profiles against measurements from the RCM and JSR experiments, it can be in-

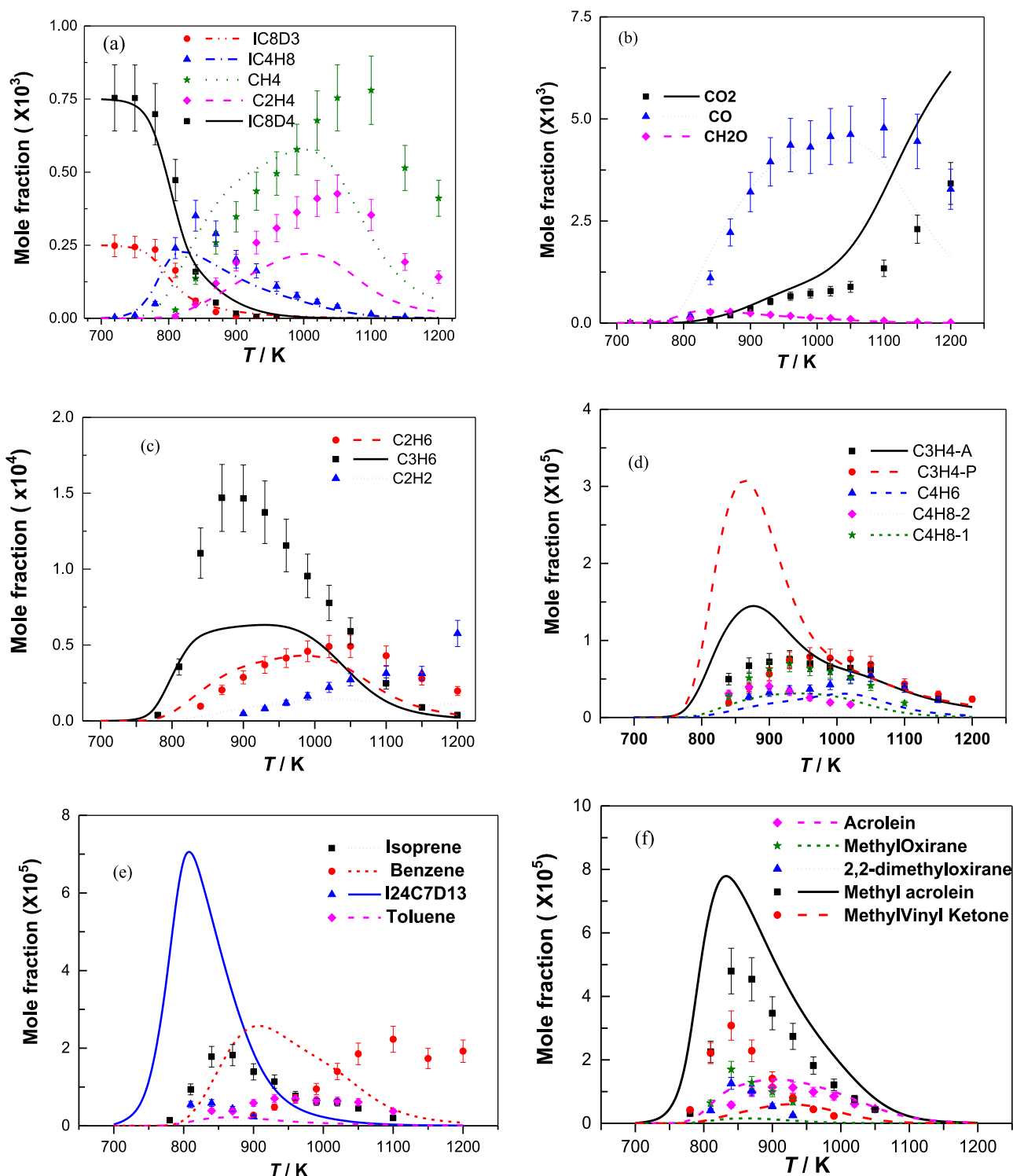


Fig. 13. Oxidation species profiles for DIB mixture containing 750 ppm DIB-1 + 250 ppm DIB-2 at $\phi = 1.0$ at 10 atm, $\tau = 0.7$ s in the JSR. Points are new experimental results, and lines represent current DIB model simulations. For clarity of species nomenclature, please refer to the dictionary provided in the supplemental material.

ferred that the mechanism performs adequately in capturing the fuel conversion profiles and formation of the global oxidation products (H_2O , CO , CO_2) and major intermediates (e.g.: iso-butene, methane, ethylene) with discrepancies in mole fractions being largely within a factor of two. The comparison of the IDTs also shows a similar level of adequate mechanism performance in predicting the global reactivity. However, significant discrepancies are observed when comparing the experimental and simulated pro-

files of some intermediates such as 2,4-dimethyl-1,3-pentadiene (I24C7D13), isoprene, benzene and toluene. These discrepancies in both global reactivity and the formation of some of the intermediates may be due to three reasons. First, we rely heavily on analogies to the oxidation of smaller hydrocarbons to develop the mechanism due to the lack of targeted experimental studies on reactions of the fuel with reactive radicals (such as H , $\dot{\text{O}}\text{H}$ and $\text{H}\dot{\text{O}}_2$) and the reactions of iso-olefin radicals. The approach of using

analogies, as shown here, helps in developing a mechanism which can reasonably predict the global reactivity trends and the speciation measurements. But some differences might be unavoidable due to the intrinsic uncertainties arising by using kinetic information from smaller molecules which often are not heavily branched. Thus, to close the gap between the experiments and modeling efforts, additional reactions might be needed. Examples of the reactions which could improve the performance of the mechanism include exploration of the low temperature chemistry of allylic peroxy radicals producing QOOH-like radicals, and olefin KHP through the reaction sequences (2)→(10)→(12)→(14)→(15), unimolecular reactions of allylic-QOOH radicals: IC8D4OOH3-1R (18), decomposition reactions of allylic radicals (IC8D3-5R (2) →I24C7D13 (8) + CH₃) and addition/abstraction reactions of DIB isomers with OH, HO₂ and CH₃O₂ radicals (see Fig. 5 for numbered reactions). The lack of accurate thermochemistry of intermediates may be another important reason for these discrepancies. Finally, iso-olefin chemistry leads to the formation of diene intermediates (e.g.: dimethyl- pentadiene, dimethyl-butadiene and isoprene) in significant amounts, and our current understanding of diene chemistry is known to be severely lacking. We believe more robust models for DIB and other iso-olefins could be improved further if dedicated studies exploring the aforementioned three reasons are performed.

It should be noted that some of the studies in the literature have focused on accurate estimations of the thermochemistry of DIB related species [55,56], reactions of DIB with OH radicals and decomposition reactions of DIB radicals [57–61], but we did not adopt the kinetics from these studies for several reasons. The thermochemistry was not adopted as the thermochemistry of only a select set of species were computed and the thermochemistry of several important species (and species classes) were not considered. Adopting the thermochemistry of the species available would disturb the internal consistency of the mechanism in capturing the thermochemistry. With regard to the reactions of DIB with OH, we found severe discrepancies between rates for H-atom abstraction reactions by OH radicals from the ab-initio studies which are shown as Supplementary material. We also did not adopt the rates for the decomposition of DIB radicals as the rate parameters provided by the study was limited to narrow temperature ranges (eg: 500 – 800 K or 500 – 1000 K) as shown in the Supplementary material. Furthermore, the quality of the fits could also be improved significantly.

6. Conclusions

DIB is one of the six fuel blendstocks short-listed for Co-Optima research [3]. DIB isomers are also important intermediates in the oxidation of iso-octane; however, typical low-temperature kinetics is limited in the existing literature DIB mechanisms. Major discrepancies were noted in the IDT predictions of various literature surrogate models when compared against the new DIB-1 data from this study. This study presents a wide range of low temperature and high-pressure experimental measurements, which can be a direct validation target for multi-component surrogate models featuring DIB-1 and/or DIB-2. A kinetic model has been developed which can adequately reproduce the observed autoignition behavior and species mole-fraction profiles.

DIB-2 shows higher reactivity in comparison to DIB-1 for the conditions considered in this study. The influence of the position of the double bond for DIB was analysed via kinetic analyses performed at 800 K and 20 atm shows that the (i) fate of the DIB alkyl radical (β -scission or reaction with O₂) and (ii) abstraction reactions (followed by reactions with hydroperoxyl radicals) are the major reaction channels that determine reactivity at these conditions. The current model can well capture the global reactivity targets of the DIB isomers, including IDTs from two independent RCM

facilities and local reactivity targets such as species profile measurements from a RCM and a JSR at various conditions. Our model is in adequate agreement with many of the stable intermediates formed in the RCM sampling experiments and in the JSR experiments performed for the DIB isomers. However, the model needs further investigation to improve the various radical addition pathways to the double-bond and H-atom abstraction reactions highlighted previously. These reaction classes are suitable candidates for future work.

Declaration of Competing Interest

The authors declare that they have no known competing financial interests or personal relationships that could have appeared to influence the work reported in this paper.

Disclaimer

This report was prepared as an account of work sponsored by an agency of the United States Government. Neither the United States Government nor any agency thereof, nor any of their employees, makes any warranty, express or implied, or assumes any legal liability or responsibility for the accuracy, completeness, or usefulness of any information, apparatus, product, or process disclosed or represents that its use would not infringe privately owned rights. Reference herein to any specific commercial product, process, or service by trade name, trademark, manufacturer, or otherwise does not necessarily constitute or imply its endorsement, recommendation, or favoring by the United States Government or any agency thereof. The views and opinions of authors expressed herein do not necessarily state or reflect those of the United States Government or any agency thereof.

Acknowledgments

The authors at NUI Galway recognize funding support from Science Foundation Ireland (SFI) via project numbers 15/IA/3177 and 16/SP/3829. The work at LLNL was performed under the auspices of the U.S. Department of Energy (DOE) by Lawrence Livermore National Laboratory under Contract DE-AC52-07NA27344 and was conducted as part of the Co-Optimization of Fuels & Engines (Co-Optima) initiative sponsored by the DOE Office of Energy Efficiency and Renewable Energy (EERE), Bioenergy Technologies and Vehicle Technologies Offices. Work at the National Renewable Energy Laboratory was performed under Contract No. DE347AC36-99G010337 as part of the Co-Optimization of Fuels & Engines (Co-Optima) initiative sponsored by the DOE Office of Energy Efficiency and Renewable Energy (EERE), Bioenergy Technologies and Vehicle Technologies Offices. This research performed in ULille was funded by TotalEnergies OneTech and is a contribution to the CPER research project Climibio. HS and GV thank the Région Hauts-de-France, and the Ministère de l'Enseignement Supérieur et de la Recherche (CPER Climibio), and the European Fund for Regional Economic Development for their financial support. CNRS Orléans received support from the CAPRYSSSE project (ANR- 11-LABX-006-01) funded by the PIA (Programme d'Investissement d'Avenir). The study was supported by the grant from the Russian Science Foundation (project No. 19-79-00325). The authors would also like to acknowledge the financial support from the Energy Agency via the Centre for Combustion Science and Technology [Project KC-CECOST 22538-4], Sweden. M.S., A.B, and P.H acknowledge funding by the Swiss Federal Office of Energy (SI/501269-01). The pyrolysis measurements (presented in Part II) were carried out at the VUV (xO4db) beamline of the Swiss Light Source storage ring, located at Paul Scherrer Institute in Villigen (Switzerland).

Supplementary materials

Supplementary material associated with this article can be found, in the online version, at doi:[10.1016/j.combustflame.2022.112301](https://doi.org/10.1016/j.combustflame.2022.112301).

References

- [1] W.K. Metcalfe, W.J. Pitz, H.J. Curran, J.M. Simmie, C.K. Westbrook, The development of a detailed chemical kinetic mechanism for diisobutylene and comparison to shock tube ignition times, *Proc. Combust. Inst.* 31 (2007) 377–384.
- [2] J. Farrell, J. Holladay, R. Wagner, Fuel Blendstocks with the Potential to Optimize Future Gasoline Engine Performance: Identification of five Chemical Families for Detailed Evaluation, US Department of Energy, Washington, DC, doi: <https://doi.org/10.2172/1434413> (2018).
- [3] D.J. Gaspar, B.H. West, D. Ruddy, T.J. Wilke, E. Polikarpov, T.L. Alleman, A. George, E. Monroe, R.W. Davis, D. Vardon, Top Ten Blendstocks Derived From Biomass For Turbocharged Spark Ignition Engines: Bio-Blendstocks With Potential for Highest Engine Efficiency, Pacific Northwest National Lab.(PNNL), Richland, WA (United States), doi: <https://doi.org/10.2172/1567705> (2019).
- [4] J. Farrell, R. Wagner, C. Moen, D. Gaspar, A Transportation Future with Science in the Driver's Seat: Mapping a Viable Route Forward for Affordable, Efficient, and Clean Fuels and Engines, 2020 DOE/EERE-2046.
- [5] J.C.G. Andrae, R.A. Head, HCCI experiments with gasoline surrogate fuels modeled by a semidetailed chemical kinetic model, *Combust. Flame* 156 (2009) 842–851.
- [6] L.R. Cancino, M. Fikri, A.A.M. Oliveira, C. Schulz, Ignition delay times of ethanol-containing multi-component gasoline surrogates: shock-tube experiments and detailed modeling, *Fuel* 90 (2011) 1238–1244.
- [7] M. Fikri, J. Herzler, R. Starke, C. Schulz, P. Roth, G.T. Kalghatgi, Autoignition of gasoline surrogates mixtures at intermediate temperatures and high pressures, *Combust. Flame* 152 (2008) 276–281.
- [8] E. Hu, G. Yin, Z. Gao, Y. Liu, J. Ku, Z. Huang, Experimental and kinetic modeling study on 2,4,4-trimethyl-1-pentene ignition behind reflected shock waves, *Fuel* 195 (2017) 97–104.
- [9] H. Li, Y. Qiu, Z. Wu, S. Wang, X. Lu, Z. Huang, Ignition delay of diisobutylene-containing multicomponent gasoline surrogates: shock tube measurements and modeling study, *Fuel* 235 (2019) 1387–1399.
- [10] B.J. Zhong, D. Zheng, A chemical mechanism for ignition and oxidation of multi-component gasoline surrogate fuels, *Fuel* 128 (2014) 458–466.
- [11] J.C.G. Andrae, Development of a detailed kinetic model for gasoline surrogate fuels, *Fuel* 87 (2008) 2013–2022.
- [12] J.C.G. Andrae, T. Kovács, Evaluation of adding an olefin to mixtures of primary reference fuels and toluene to model the oxidation of a fully blended gasoline, *Energy Fuels* 30 (2016) 7721–7730.
- [13] S. Ren, S.L. Kokjohn, Z. Wang, H. Liu, B. Wang, J. Wang, A multi-component wide distillation fuel (covering gasoline, jet fuel and diesel fuel) mechanism for combustion and PAH prediction, *Fuel* 208 (2017) 447–468.
- [14] M. Mehl, W.J. Pitz, C.K. Westbrook, K. Yasunaga, C. Conroy, H.J. Curran, Autoignition behavior of unsaturated hydrocarbons in the low and high temperature regions, *Proc. Combust. Inst.* 33 (2011) 201–208.
- [15] G. Mittal, C.J. Sung, Homogeneous charge compression ignition of binary fuel blends, *Combust. Flame* 155 (2008) 431–439.
- [16] Y. Wu, M. Yang, X. Yao, Y. Liu, C. Tang, Comparative studies on the ignition characteristics of diisobutylene isomers and iso-octane by using a rapid compression machine, *Fuel* 276 (2020) 118008.
- [17] H. Song, R. Dauphin, G. Vanhove, A kinetic investigation on the synergistic low-temperature reactivity, antagonistic RON blending of high-octane fuels: diisobutylene and cyclopentane, *Combust. Flame* 220 (2020) 23–33.
- [18] N. Lokachari, S. Panigrahy, G. Kukkadapu, G. Kim, S.S. Vasu, W.J. Pitz, H.J. Curran, The influence of iso-butene kinetics on the reactivity of di-isobutylene and iso-octane, *Combust. Flame* 222 (2020) 186–195.
- [19] N. Lokachari, G. Kukkadapu, B.D. Etz, G.M. Fioroni, S. Kim, M. Steglich, A. Bodi, P. Hemberger, S.S. Matveev, A. Thomas, H. Song, G. Vanhove, K. Zhang, G. Dayma, M. Lailliau, Z. Serinyel, A.A. Konnov, P. Dagaut, W.J. Pitz, H.J. Curran, A comprehensive experimental and kinetic modeling study of di-isobutylene isomers: Part 2, Under revision (2022).
- [20] C. Morley, Gaseq, 2004 Available at <http://www.gaseq.co.uk>.
- [21] Y. Fenard, M.A. Boumehdi, G. Vanhove, Experimental and kinetic modeling study of 2-methyltetrahydrofuran oxidation under engine-relevant conditions, *Combust. Flame* 178 (2017) 168–181.
- [22] Y. Fenard, H. Song, H. Minwegen, P. Parab, C. Sampaio Mergulhão, G. Vanhove, K.A. Heufer, 2,5-Dimethyltetrahydrofuran combustion: ignition delay times at high and low temperatures, speciation measurements and detailed kinetic modeling, *Combust. Flame* 203 (2019) 341–351.
- [23] C.S. Mergulhão, H.-H. Carstensen, H. Song, S.W. Wagnon, W.J. Pitz, G. Vanhove, Probing the antiknock effect of anisole through an ignition, speciation and modeling study of its blends with isooctane, *Proc. Combust. Inst.* 38 (1) (2021) 739–748.
- [24] D. Lee, S. Hochgreb, Rapid compression machines: heat transfer and suppression of corner vortex, *Combust. Flame* 114 (1998) 531–545.
- [25] N. Bourgeois, S.S. Goldsborough, H. Jeanmart, F. Contino, CFD simulations of Rapid Compression Machines using detailed chemistry: evaluation of the 'crevice containment' concept, *Combust. Flame* 189 (2018) 225–239.
- [26] S.S. Goldsborough, S. Hochgreb, G. Vanhove, M.S. Wooldridge, H.J. Curran, C.J. Sung, Advances in rapid compression machine studies of low- and intermediate-temperature autoignition phenomena, *Prog. Energy Combust. Sci.* 63 (2017) 1–78.
- [27] G. Vanhove, M. Ribaucour, R. Minetti, On the influence of the position of the double bond on the low-temperature chemistry of hexenes, *Proc. Combust. Inst.* 30 (2005) 1065–1072.
- [28] J.T. Scanlon, D.E. Willis, Calculation of flame ionization detector relative response factors using the effective carbon number concept, *J. Chromatogr. Sci.* 23 (1985) 333–340.
- [29] P. Dagaut, M. Cathonnet, J.P. Rouan, R. Foulatier, A. Quilgars, J.C. Boettner, F. Gaillard, H. James, A jet-stirred reactor for kinetic studies of homogeneous gas-phase reactions at pressures up to ten atmospheres (≈ 1 MPa), *J. Phys. E Sci. Instrum.* 19 (1986) 207–209.
- [30] J. Bugler, B. Marks, O. Mathieu, R. Archuleta, A. Camou, C. Grégoire, K.A. Heufer, E.L. Petersen, H.J. Curran, An ignition delay time and chemical kinetic modeling study of the pentane isomers, *Combust. Flame* 163 (2016) 138–156.
- [31] K. Zhang, C. Banyon, U. Burke, G. Kukkadapu, S.W. Wagnon, M. Mehl, H.J. Curran, C.K. Westbrook, W.J. Pitz, An experimental and kinetic modeling study of the oxidation of hexane isomers: developing consistent reaction rate rules for alkanes, *Combust. Flame* 206 (2019) 123–137.
- [32] R. Fang, G. Kukkadapu, M. Wang, S.W. Wagnon, K. Zhang, M. Mehl, C.K. Westbrook, W.J. Pitz, C.-J. Sung, Fuel molecular structure effect on autoignition of highly branched iso-alkanes at low-to-intermediate temperatures: iso-octane versus iso-dodecane, *Combust. Flame* 214 (2020) 152–166.
- [33] E.R. Ritter, THERM: a computer code for estimating thermodynamic properties for species important to combustion and reaction modeling, *J. Chem. Inf. Comput. Sci.* 31 (1991) 400–408.
- [34] Y. Li, H.J. Curran, Extensive theoretical study of the thermochemical properties of unsaturated hydrocarbons and allylic and super-allylic radicals: the development and optimization of group additivity values, *J. Phys. Chem. A* 122 (2018) 4736–4749.
- [35] S.M. Burke, J.M. Simmie, H.J. Curran, Critical evaluation of thermochemical properties of C1–C4 Species: updated group-contributions to estimate thermochemical properties, *J. Phys. Chem. Ref. Data* 44 (2015) 013101.
- [36] C. Cavallotti, F. Leonori, N. Balucani, V. Nevrlý, A. Bergeat, S. Falcinelli, G. Vanuzzo, P. Casavecchia, Relevance of the channel leading to formaldehyde + triplet ethylidene in the O(3P) + propene reaction under combustion conditions, *J. Phys. Chem. Lett.* 5 (2014) 4213–4218.
- [37] J. Zádor, S.J. Klippenstein, J.A. Miller, Pressure-dependent OH yields in Alkene + HO₂ reactions: a theoretical study, *J. Phys. Chem. A* 115 (2011) 10218–10225.
- [38] J. Badra, F. Khaled, B.R. Giri, A. Farooq, A shock tube study of the branching ratios of propene + OH reaction, *Phys. Chem. Chem. Phys.* 17 (2015) 2421–2431.
- [39] S.S. Vasu, L.K. Huynh, D.F. Davidson, R.K. Hanson, D.M. Golden, Reactions of OH with Butene Isomers: measurements of the Overall Rates and a Theoretical Study, *J. Phys. Chem. A* 115 (2011) 2549–2556.
- [40] C.W. Zhou, J.M. Simmie, K.P. Somers, C.F. Goldsmith, H.J. Curran, Chemical kinetics of hydrogen atom abstraction from allylic sites by ³O₂; implications for combustion modeling and simulation, *J. Phys. Chem. A* 121 (2017) 1890–1899.
- [41] J. Badra, A. Farooq, Site-specific reaction rate constant measurements for various secondary and tertiary H-abstraction by OH radicals, *Combust. Flame* 162 (2015) 2034–2044.
- [42] R. Sivaramakrishnan, J.V. Michael, Rate constants for OH with selected large alkanes: shock-tube measurements and an improved group scheme, *J. Phys. Chem. A* 113 (2009) 5047–5060.
- [43] K. Wang, S.M. Villano, A.M. Dean, The impact of resonance stabilization on the intramolecular hydrogen-atom shift reactions of hydrocarbon radicals, *ChemPhysChem* 16 (2015) 2635–2645.
- [44] Y. Li, C.W. Zhou, K.P. Somers, K. Zhang, H.J. Curran, The oxidation of 2-butene: a high pressure ignition delay, kinetic modeling study and reactivity comparison with isobutene and 1-butene, *Proc. Combust. Inst.* 36 (2017) 403–411.
- [45] D. Schleier, P. Constantinidis, N. Faßheber, I. Fischer, G. Friedrichs, P. Hemberger, E. Reusch, B. Sztáray, K. Voronova, Kinetics of the a-C₃H₅ + O₂ reaction, investigated by photoionization using synchrotron radiation, *Phys. Chem. Chem. Phys.* 20 (2018) 10721–10731.
- [46] D. Schleier, E. Reusch, M. Gerlach, T. Preitschopf, D.P. Mukhopadhyay, N. Faßheber, G. Friedrichs, P. Hemberger, I. Fischer, Kinetics of 1- and 2-methylallyl + O₂ reaction, investigated by photoionisation using synchrotron radiation, *Phys. Chem. Chem. Phys.* 23 (2021) 1539–1549.
- [47] C.J. Chen, J.W. Bozzelli, Thermochemical property, pathway and kinetic analysis on the reactions of allylic isobutenyl radical with O₂: an elementary reaction mechanism for isobutene oxidation, *J. Phys. Chem. A* 104 (2000) 9715–9732.
- [48] K. Zhang, C. Banyon, J. Bugler, H.J. Curran, A. Rodriguez, O. Herbinet, F. Battin-Leclerc, C. B'Chir, K.A. Heufer, An updated experimental and kinetic modeling study of n-heptane oxidation, *Combust. Flame* 172 (2016) 116–135.
- [49] X. Sun, W. Zong, J. Wang, Z. Li, X. Li, Pressure-dependent rate rules for cycloaddition, intramolecular H-shift, and concerted elimination reactions of alkenyl peroxy radicals at low temperature, *Phys. Chem. Chem. Phys.* 21 (2019) 10693–10705.
- [50] C.F. Goldsmith, W.H. Green, S.J. Klippenstein, Role of O₂ + QOOH in low-temperature ignition of propane. 1. Temperature and pressure dependent rate coefficients, *J. Phys. Chem. A* 116 (2012) 3325–3346.

- [51] C.W. Zhou, Y. Li, E. O'Connor, K.P. Somers, S. Thion, C. Keese, O. Mathieu, E.L. Petersen, T.A. DeVerter, M.A. Oehlschlaeger, G. Kukkadapu, C.J. Sung, M. Alrefae, F. Khaled, A. Farooq, P. Dirrenberger, P.A. Glaude, F. Battin-Leclerc, J. Santner, Y. Ju, T. Held, F.M. Haas, F.L. Dryer, H.J. Curran, A comprehensive experimental and modeling study of isobutene oxidation, *Combust. Flame* 167 (2016) 353–379.
- [52] J. Zádor, A.W. Jasper, J.A. Miller, The reaction between propene and hydroxyl, *Phys. Chem. Chem. Phys.* 11 (2009) 11040–11053.
- [53] H. Sun, J.W. Bozzelli, C.K. Law, Thermochemical and kinetic analysis on the reactions of O₂ with products from OH addition to isobutene, 2-hydroxy-1,1-dimethylethyl, and 2-hydroxy-2-methylpropyl radicals: HO₂ formation from oxidation of neopentane, Part II, *J. Phys. Chem. A* 111 (2007) 4974–4986.
- [54] K. Wang, S.M. Villano, A.M. Dean, Experimental and kinetic modeling study of butene isomer pyrolysis: Part II. Isobutene, *Combust. Flame* 176 (2017) 23–37.
- [55] S. Dong, K. Zhang, P.K. Senecal, G. Kukkadapu, S.W. Wagnon, S. Barrett, N. Lokachari, S. Panigaphy, W.J. Pitz, H.J. Curran, A comparative reactivity study of 1-alkene fuels from ethylene to 1-heptene, *Proc. Combust. Inst.* 38 (2021) 611–619.
- [56] X. Zhang, C. Cao, J. Zou, Y. Li, Y. Zhang, Q.Xu J.Guo, B. Feng, S.M. Sarathy, J. Yang, Z. Wang, F. Qi, Y. Li, Low-temperature oxidation chemistry of 2,4,4-trimethyl-1-pentene (diisobutylene) triggered by dimethyl ether (DME): a jet-stirred reactor oxidation and kinetic modeling investigation, *Combust. Flame* 234 (2021) 111629.
- [57] G. Yin, E. Hu, M. Zhou, H. Zhan, Z. Huang, Kinetic study on the isomerization and decomposition of the alkenyl radicals of 2,4,4-trimethyl-1-pentene, *Energy Fuels* 34 (11) (2020) 14757–14767.
- [58] G. Yin, E. Hu, X. Li, J. Ku, Z. Gao, Z. Huang, Theoretical study of abstraction and addition reactions of 2,4,4-trimethyl-1-pentene with H and O(³P) Radical, *Energy Fuels* 32 (11) (2018) 11831–11842 Chemically activated reaction pathways from H-addition reactions are missing. These reactions have been shown to be important for many olefins. For this reason we did not use these rates.
- [59] G. Yin, E. Hu, Z. Gao, F. Yang, Z. Huang, Kinetics of H abstraction and addition reactions of 2,4,4-trimethyl-2-pentene by OH radical, *Chem. Phys. Lett.* 696 (2018) 125–134.
- [60] G. Yin, E. Hu, F. Yang, J. Ku, Z. Huang, Kinetics of H abstraction and addition reactions of 2,4,4-trimethyl-1-pentene by OH radical, *Fuel* 210 (2017) 646–658.
- [61] G. Yin, Z. Gao, E. Hu, Z. Xu, Z. Huang, Comprehensive experimental and kinetic study of 2,4,4-trimethyl-1-pentene oxidation, *Combust. Flame* 208 (2019) 246–261.